medRxiv preprint doi: https://doi.org/10.1101/2020.08.04.20168013; this version posted September 10, 2020. The copyright holder for this preprint (which was not certified by peer review) is the author/funder, who has granted medRxiv a license to display the preprint in perpetuity.
It is made available under a CC-BY-NC-ND 4.0 International license .

Analysis of COVID-19 and comorbidity co-infection Model with Optimal Control

A. Omame[1,†], N. Sene[2], I. Nometa[3], C. I. Nwakanma[4], E. U. Nwafor[1], N. O. Iheonu[1], D. Okuonghae[5]

Abstract

The new coronavirus disease 2019 (COVID-19) infection is a double challenge for people infected with comorbidities such as cardiovascular and cerebrovascular diseases and diabetes. Comorbidities have been reported to be risk factors for the complications of COVID-19. In this work, we develop and analyze a mathematical model for the dynamics of COVID-19 infection in order to assess the impacts of prior comorbidity on COVID-19 complications and COVID-19 re-infection. The model is simulated using data relevant to the dynamics of the diseases in Lagos, Nigeria, making predictions for the attainment of peak periods in the presence or absence of comorbidity. The model is shown to undergo the phenomenon of backward bifurcation caused by the parameter accounting for increased susceptibility to COVID-19 infection by comorbid susceptibles as well as the rate of re-infection by those who have recovered from a previous COVID-19 infection. Sensivity analysis of the model when the population of individuals co-infected with COVID-19 and comorbidity is used as response function revealed that the top ranked parameters that drive the dynamics of the co-infection model are the effective contact rate for COVID-19 transmission, β_{CV}, the parameter accounting for increased sucseptibility to COVID-19 by comorbid susceptibles, χ_{CM}, the comorbidity development rate, θ_{CM}, the detection rate for singly infected and co-infected individuals, η_1 and η_2, as well as the recovery rate from COVID-19 for co-infected individuals, φ_{I2}. Simulations of the model reveal that the cumulative confirmed cases (without comorbidity) may get up to 180,000 after 200 days, if the hyper susceptibility rate of comorbid susceptibles is as high as 1.2 per day. Also, the cumulative confirmed cases (including those co-infected with comorbidity) may be as high as 1000,000 cases by the end of November, 2020 if the re-infection rates for COVID-19 is 0.1 per day. It may be worse than this if the re-infection rates increase higher. Moreover, if policies are strictly put in place to step down the probability of COVID-19 infection by comorbid susceptibles to as low as 0.4 per day and step up the detection rate for singly infected individuals to 0.7 per day, then the reproduction number can be brought very low below one, and COVID-19 infection eliminated from the population. In addition, optimal control and cost-effectiveness analysis of the model reveal that the the strategy that prevents COVID-19 infection by comorbid susceptibles has the least ICER and is the most cost-effective of all the control strategies for the prevention of COVID-19.

Keywords: COVID-19, Comorbidity, Re-infection, Data-fitting, Optimal Control.

[1] Department of Mathematics, Federal University of Technology Owerri, Nigeria
[2] Laboratoire Lmdan, Département de Mathématiques de la Décision, Université Cheikh Anta Diop de Dakar, Facultédes Sciences Economiques et Gestion, BP 5683 Dakar Fann, Senegal
[3] Department of Mathematics, University of Hawaii Manoa, USA
[4] Networked Systems Lab, IT Covergence Engineering, School of Electronic Engineering, Kumoh National Institute of Technology Gumi, Korea
[5] Department of Mathematics, University of Benin, Benin City, Nigeria
[†]Corresponding author: omame2020@gmail.com, andrew.omame@futo.edu.ng

NOTE: This preprint reports new research that has not been certified by peer review and should not be used to guide clinical practice.

medRxiv preprint doi: https://doi.org/10.1101/2020.08.04.20168013; this version posted September 10, 2020. The copyright holder for this preprint (which was not certified by peer review) is the author/funder, who has granted medRxiv a license to display the preprint in perpetuity.
It is made available under a CC-BY-NC-ND 4.0 International license .

1 Introduction

The new coronavirus disease 2019 (COVID-19) was reported for the first time in the Chinese city of Wuhan, in the closing month of the year 2019 [22]. The disease spread rapidly across the globe like wildfire, that on March 11, 2020, the World Health Organization (WHO) delared it a global pandemic [11]. As of 25th July, 2020, the global cases of COVID-19 infection stands at 15,762,007 with 640,276 deaths [12]. The morbidity and mortality vary across countries of the world with the highest reported in the United States (4,113,224 confirmed cases with 145,556 deaths), and Brazil (2,287,475 confirmed cases with 85,238 deaths) as of 25th July, 2020. [12]. COVID-19 "can often present as a common cold-like illness", with other symptoms including fever, fatigue, muscle pains, loss or change of taste or smell, shortness of breath, dry cough and sore throat [47].

The disease can be spread from person-to-person through the breathing in of respiratory droplets from infected persons and via direct contact with contaminated objects and surfaces [2]. Although no vaccine or antiviral treatments have been approved for the prevention or management of COVID-19, governments of different nations and individuals have embarked on non-pharmaceutical interventions such as face-mask usage in public places, social disancing observance and lockdown imposition as a means of effectively reducing the spread of the disease [4, 42]. Epidemiological studies have recently pointed towards the need to consider COVID-19 and comorbidity (such as diabetes, lung disease and heart disease) co-infection, as those with the latter have a higher chance of infection with the former [11]. Bjorgul *et al.* [6] defined comorbidities as "diseases or medical conditions unrelated in etiology or causality to the principal diagnosis that coexist with the disease of interest". According to the Centres for Disease Control and prevention (CDC), "People of any age with the following conditions are at increased risk of severe illness from COVID-19: Chronic kidney disease, COPD (chronic obstructive pulmonary disease), Immunocompromised state (weakened immune system) from solid organ transplant, Obesity (body mass index [BMI] of 30 or higher), Serious heart conditions, such as heart failure, coronary artery disease, or cardiomyopathies, Sickle cell disease, Type 2 diabetes mellitus, Hypertension or high blood pressure and Neurologic conditions, such as dementia" [10]. This is further confirmed by a clinical report by Huang *et al.* [18] who in a survey of 41 confirmed COVID-19 patients discovered that thirteen of them had underlying diseases, which include, hypertension, chronic obstructive pulmonary disease cardiovascular disease and diabetes. Furthermore, Wang *et al.* reported from a finding incolving 138 patients, that over 45% of them had one or more comorbidities and that "the patients who were admitted to the intensive care unit (ICU) had a higher number of comorbidities (72.2%) than those not admitted to the ICU (37.3%)" [46, 49]. In Nigeria, the Ministry of Health had reported that prior comorbid conditions such as diabetes mellitus, tuberculosis and hypertension were responsible for about 70% of COVID-19 related deaths [38]. Recent studies carried out in Nigeria estimated the prevalence of diabetes mellitus (DM) to range from lowest level of 0.8% among adults in rural settings to over 7% in urban Lagos with an average of 2.2% nationally [15]. Diabetes mellitus has been reported to increase the vulnerability of individuals to infection with COVID-19 in Nigeria. The prevalence of DM is higher in patients with severe COVID-19 disease than in patients with mild symptoms [33]. More recently, WHO has warned that currently no evidence to show that those who have recovered from COVID-19 infection can not get re-infected [48]. On April 13, 2020, South Korea reported that more than 100 of its recovered cases of COVID-19 have been re-infected again [41]. This calls for serious concern as several countries, including China and South Korea, which had previously recorded giant strides in curbing the the virus, have recently reported second waves of COVID-19 infections [5, 14].

Mathematical modelling has been a powerful means of studying the behaviour of infectious diseases [13, 30, 31, 34, 35, 36, 40, 39, 43]. A lot of models have been developed for the dynamics of COVID-19 [1, 16, 19, 20, 21, 28, 32]. In this study, we shall be investigating the impact of re-infection and co-infection with comorbidity on the dynamics of COVID-19 disease. In addition, we shall be carrying out optimal control analysis on the model to assess the impact of some control strategies on the prevention of COVID-19. Specifically, the comorbidity of interest for this study shall be **diabetes mellitus**.

The paper is organized as follows. The model formulation and basic properties of the model are reported in Section 2. The model (without controls) is analyzed (qualitatively and quantitatively) in Sections 3 and 4. Optimal control analysis is carried out in Section 5 while Section 6 gives the concluding remarks.

medRxiv preprint doi: https://doi.org/10.1101/2020.08.04.20168013; this version posted September 10, 2020. The copyright holder for this preprint (which was not certified by peer review) is the author/funder, who has granted medRxiv a license to display the preprint in perpetuity.
It is made available under a CC-BY-NC-ND 4.0 International license .

2 Model formulation

The total population at time t, denoted by $N_{\text{H}}(t)$, is divided into eight mutually-exclusive compartments: Susceptible individuals ($S_{\text{H}}(t)$), comorbid susceptible individuals (S_{CM}), individuals with COVID-19 infection ($I_{\text{CV}}(t)$), isolated and hospitalized individuals infected with COVID-19 ($Q_{\text{CV}}(t)$), individuals who have recovered from COVID-19 infection ($R_{\text{CV}}(t)$), individuals co-infected with COVID-19 and comorbidity ($I_{\text{CVCM}}(t)$), isolated and hospitalized individuals co-infected with COVID-19 infection and comorbidity (Q_{CVCM}), individuals who have recovered from COVID-19 infection but with comorbidity (R_{CM}). Susceptible individuals acquire COVID-19 infection at the rate

$$\lambda_{\text{CV}} = \frac{\beta_{\text{CV}}(I_{\text{CV}} + \sigma_{\text{CM}} I_{\text{CVCM}})}{N_{\text{H}}},$$

where σ_{CM} accounts for increased infectiousness of co-infected individuals. Furthermore, susceptible individuals also acquire comorbidity at the rate θ_{CM}. Comorbid susceptible individuals acquire COVID-19 infection at an increased rate $\chi_{\text{CM}}\lambda_{\text{CV}}$, with $\chi_{\text{CM}} > 1$. Natural death occurs in all compartments at the rate μ_{H}. It is imperative to state at the onset that the comorbidity considered in this study is **diabetes mellitus**.
The total population at time, t is given by

$$N_{\text{H}} = S_{\text{H}} + S_{\text{CM}} + I_{\text{CV}} + Q_{\text{CV}} + R_{\text{CV}} + I_{\text{CVCM}} + Q_{\text{CVCM}} + R_{\text{CVCM}}$$

Based on the above formulations and assumptions, the COVID-19 and comorbidity co-infection model is given by the system of non-linear deterministic differential equations (flow diagram of the model is shown in Figure 1, the associated state variables and parameters are well described in Table 1) given below:

Table 1: Description of variables and parameters in the model equation

Variable	**Interpretation**
S_{H}	Susceptible humans
S_{CM}	Comorbid susceptible individuals
I_{CV}	Individuals singly infected with COVID-19
Q_{CV}	infectious individuals isolated and hospitalized for COVID-19 treatment
R_{CV}	Individuals who have recovered from COVID-19 infection
I_{CVCM}	Individuals co-infected with COVID-19 and comorbidity
Q_{CVCM}	Isolated and hospitalized individuals co-infected with COVID-19 and comorbidity
R_{CM}	Individuals who have recovered from COVID-19 but with comorbidity
Parameter	**Interpretation**
Λ_{H}	Recruitment rate
μ_{H}	Natural death rate
β_{CV}	Effective contact rate for COVID-19 tranmission
θ_{CM}	Rate of comorbidity development by susceptible humans
η_1, η_2	Detection rates for compartments I_{CV} and I_{CVCM}, respectively
$\varphi_{\text{I1}}, \varphi_{\text{Q1}}, \varphi_{\text{I2}}, \varphi_{\text{Q2}}$	Recovery rates from COVID-19 for individuals in compartments $I_{\text{CV}}, Q_{\text{CV}}, I_{\text{CVCM}}$ and Q_{CVCM}, respectively
δ_1	COVID-19-induced death rate for infected individuals in I_{CV} and Q_{CV} compartments, respectively
δ_2	comorbidity-induced death rate for infected individuals in I_{CVCM} compartment
ψ_1, ψ_2	Re-infection rates for individuals who have recovered from COVID-19 in compartments R_{CV} and R_{CM}
σ_{CM}	Modification parameter for increased infectiousness of co-infected individuals due to presence of comorbidity
χ_{CM}	modification parameter accounting for increased susceptibility to COVID-19 infection by comorbid susceptibles

medRxiv preprint doi: https://doi.org/10.1101/2020.08.04.20168013; this version posted September 10, 2020. The copyright holder for this preprint **(which was not certified by peer review)** is the author/funder, who has granted medRxiv a license to display the preprint in perpetuity.
It is made available under a CC-BY-NC-ND 4.0 International license .

$$
\begin{aligned}
\frac{dS_{\text{H}}}{dt} &= \Lambda_{\text{H}} - (\lambda_{\text{CV}} + \theta_{\text{CM}} + \mu_{\text{H}})S_{\text{H}} \\
\frac{dS_{\text{CM}}}{dt} &= \theta_{\text{CM}}S_{\text{H}} - \chi_{\text{CM}}\lambda_{\text{CV}}S_{\text{CM}} - \mu_{\text{H}}S_{\text{CM}} \\
\frac{dI_{\text{CV}}}{dt} &= \lambda_{\text{CV}}S_{\text{H}} - (\eta_1 + \varphi_{\text{I1}} + \mu_{\text{H}})I_{\text{CV}} + \psi_1\lambda_{\text{CV}}R_{\text{CV}} \\
\frac{dQ_{\text{CV}}}{dt} &= \eta_1 I_{\text{CV}} - (\varphi_{\text{Q1}} + \delta_1 + \mu_{\text{H}})Q_{\text{CV}} \\
\frac{dR_{\text{CV}}}{dt} &= \varphi_{\text{I1}}I_{\text{CV}} + \varphi_{\text{Q1}}Q_{\text{CV}} - \mu_{\text{H}}R_{\text{CV}} - \psi_1\lambda_{\text{CV}}R_{\text{CV}} \\
\frac{dI_{\text{CVCM}}}{dt} &= \chi_{\text{CM}}\lambda_{\text{CV}}S_{\text{CM}} - (\eta_2 + \varphi_{\text{I2}} + \mu_{\text{H}})I_{\text{CVCM}} + \psi_2\lambda_{\text{CV}}R_{\text{CM}} \\
\frac{dQ_{\text{CVCM}}}{dt} &= \eta_2 I_{\text{CVCM}} - (\delta_1 + \delta_2 + \varphi_{\text{Q2}} + \mu_{\text{H}})Q_{\text{CVCM}} \\
\frac{dR_{\text{CM}}}{dt} &= \varphi_{\text{I2}}I_{\text{CVCM}} + \varphi_{\text{Q2}}Q_{\text{CVCM}} - \mu_{\text{H}}R_{\text{CM}} - \psi_2\lambda_{\text{CV}}R_{\text{CM}}
\end{aligned}
\tag{1}
$$

with

$$\lambda_{\text{CV}} = \frac{\beta_{\text{CV}}(I_{\text{CV}} + \sigma_{\text{CM}}I_{\text{CVCM}})}{N_{\text{H}}},$$

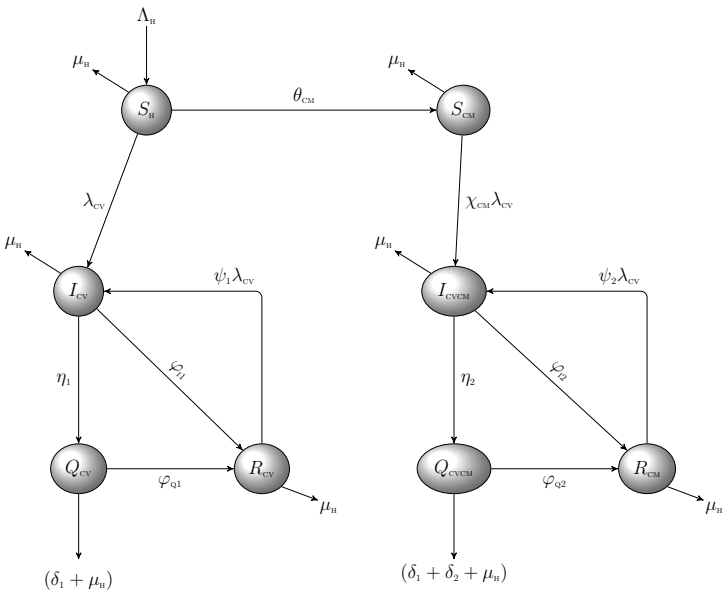

Figure 1: Schematic diagram of the model (1) where $\lambda_{\text{CV}} = \frac{\beta_{\text{CV}}(I_{\text{CV}}+\sigma_{\text{CM}}I_{\text{CVCM}})}{N_{\text{H}}}$

medRxiv preprint doi: https://doi.org/10.1101/2020.08.04.20168013; this version posted September 10, 2020. The copyright holder for this preprint (which was not certified by peer review) is the author/funder, who has granted medRxiv a license to display the preprint in perpetuity.
It is made available under a CC-BY-NC-ND 4.0 International license .

2.1 Basic properties of the model

2.1.1 Positivity and boundedness

For the model (1) to be epidemiologically meaningful, it is important to prove that all its state variables are non-negative for all time (t).

Theorem 2.1 *Let the initial data* $S_{\text{H}} > 0, S_{\text{CM}} > 0, I_{\text{CV}} > 0, Q_{\text{CV}} > 0, R_{\text{CV}} > 0, I_{\text{CVCM}} > 0, Q_{\text{CVCM}} > 0, R_{\text{CM}} > 0$. *Then the solutions* $(S_{\text{H}}, S_{\text{CM}}, I_{\text{CV}}, Q_{\text{CV}}, R_{\text{CV}}, I_{\text{CVCM}}, Q_{\text{CVCM}}, R_{\text{CM}})$ *of the model* (1) *are positive for all time* $t > 0$.

Proof. Let
$t_1 = \sup\{t > 0 : S_{\text{H}} > 0, S_{\text{CM}} > 0, I_{\text{CV}} > 0, Q_{\text{CV}} > 0, R_{\text{CV}} > 0, I_{\text{CVCM}} > 0, Q_{\text{CVCM}} > 0, R_{\text{CM}} > 0 \in [0, t]\}$. Thus, $t_1 > 0$.
We have, from the first equation of the system (1) that

$$\frac{dS_{\text{H}}}{dt} = \Lambda_{\text{H}} - (\lambda_{\text{CV}} + \theta_{\text{CM}} + \mu_{\text{H}})S_{\text{H}}$$

which can be re-written as

$$\frac{d}{dt}\left\{S_{\text{H}}(t)\exp\left[\int_0^t \lambda_{\text{CV}}(u)du + \theta_{\text{CM}}t + \mu_{\text{H}}t\right]\right\} = \Lambda_{\text{H}}\exp\left[\int_0^t \lambda_{\text{CV}}(u)du + \theta_{\text{CM}}t + \mu t\right]$$

so that

$$\frac{d}{dt}\left\{S_{\text{H}}(t_1)\exp\left[\int_0^{t_1} \lambda_{\text{CV}}(u)du + \theta_{\text{CM}}t + \mu(t)_1\right]\right\} - S_{\text{H}}(0) = \Lambda_{\text{H}}\int_0^{t_1}\exp\left[\int_0^x \lambda_{\text{CV}}(u)du + \theta_{\text{CM}}t + \mu(x)\right]dx$$

so that

$$S_{\text{H}}(t_1) = S_{\text{H}}(0)\exp\left[-\int_0^{t_1} \lambda_{\text{CV}}(u)du - \theta_{\text{CM}}t_1 - \mu t_1\right] + \exp\left[-\int_0^{t_1} \lambda_{\text{CV}}(u)du - \theta_{\text{CM}}t - \mu t_1\right]$$
$$\times\,\Lambda_{\text{H}}\int_0^{t_1}\exp\left[\int_0^x \lambda_{\text{CV}}(u)du + \theta_{\text{CM}}t + \mu(x)\right]dx > 0$$

In a similar manner, it can be proven that:
$S_{\text{CM}} > 0, I_{\text{CV}} > 0, Q_{\text{CV}} > 0, R_{\text{CV}} > 0, I_{\text{CVCM}} > 0, Q_{\text{CVCM}} > 0, R_{\text{CM}} > 0$

2.2 Invariant regions

The co-infection model (1) will be analyzed in a biologically feasible region as follows. We first show that the system (1) is dissipative in a proper subset $\mathcal{D} \subset \mathfrak{R}^8_+$. Let

$$\mathcal{D} = \left\{(S_{\text{H}}, S_{\text{CM}}, I_{\text{CV}}, Q_{\text{CV}}, R_{\text{CV}}, I_{\text{CVCM}}, Q_{\text{CVCM}}, R_{\text{CM}}) \in \mathfrak{R}^8_+ : S_{\text{H}} + S_{\text{CM}} + I_{\text{CV}} + Q_{\text{CV}} + R_{\text{CV}} + I_{\text{CVCM}} + Q_{\text{CVCM}} + R_{\text{CM}} \leq \frac{\Lambda_{\text{H}}}{\mu_{\text{H}}}\right\}$$

The following steps are followed to establish the positive invariance of $\mathcal{D}$.
Adding all the equations of the system (1) gives

$$\frac{dN_{\text{H}}}{dt} = \Lambda_{\text{H}} - \mu_{\text{H}}N_{\text{H}}(t) - [\delta_1(Q_{\text{CV}} + Q_{\text{CVCM}}) + \delta_2 Q_{\text{CVCM}}] \tag{2}$$

From (2), we have that

$$\Lambda_{\text{H}} - (\mu_{\text{H}} + 3\delta_{\text{H}})N_{\text{H}} \leq \frac{dN_{\text{H}}}{dt} < \Lambda_{\text{H}} - \mu_{\text{H}}N_{\text{H}}$$

where $\delta_{\text{H}} = \min\{\delta_1, \delta_2\}$
Using the Comparison theorem [23], we have that, $N_{\text{H}}(t) \leq \dfrac{\Lambda_{\text{H}}}{\mu_{\text{H}}}$ if $N_{\text{H}}(0) \leq \dfrac{\Lambda_{\text{H}}}{\mu_{\text{H}}}$. Thus, the region $\mathcal{D}$ is

medRxiv preprint doi: https://doi.org/10.1101/2020.08.04.20168013; this version posted September 10, 2020. The copyright holder for this preprint (which was not certified by peer review) is the author/funder, who has granted medRxiv a license to display the preprint in perpetuity.
It is made available under a CC-BY-NC-ND 4.0 International license .

positively invariant. Hence, it is sufficient to consider the dynamics of the flow generated by the system (1) in $\mathcal{D}$. Thus, within this region, the model (1) is said to be be epidemiologically and mathematically well-posed [17]. Thus, every solution of the model (1) with initial conditions in $\mathcal{D}$ remains in $\mathcal{D}$ for all time $t \geq 0$. Therefore, the $\omega-$limit sets of the system (1) are contained in $\mathcal{D}$. This result is summarized thus.

Lemma 2.1 *The region $\mathcal{D} \subset \mathfrak{R}^8_+$ is positively-invariant for the model* (1) *with initial conditions in $\mathfrak{R}^8_+$.*

3 Analysis of the model without controls

In this section, we seek to qualitatively study the dynamical properties of the model (1) without controls.

3.1 Basic reproduction number of the co-infection model (1)

The COVID-19-comorbidity co-infection model (1) has a COVID-19 free equilibrium (CFE), obtained by setting the disease classes and the right-hand sides of the equations in the model (1) to zero, given by

$$\begin{aligned}\xi_0 =&(S^*_{\text{H}}, S^*_{\text{CM}}, I^*_{\text{CV}}, Q^*_{\text{CV}}, R^*_{\text{CV}}, I^*_{\text{CVCM}}, Q^*_{\text{CVCM}}, R^*_{\text{CM}})\\ =&\Big(\frac{\Lambda_{\text{H}}}{(\mu_{\text{H}}+\theta_{\text{CM}})}, \frac{\theta_{\text{CM}}\Lambda_{\text{H}}}{\mu_{\text{H}}(\mu_{\text{H}}+\theta_{\text{CM}})}, 0,0,0,0,0,0\Big)\end{aligned} \tag{3}$$

The basic reproduction number of the co-infection model (1), using the approach illustrated in [44], is given by

$$\mathcal{R}_{0\text{C}} = \beta_{\text{CV}}\left(\frac{S^*_{\text{H}}}{N^*_{\text{H}}(\eta_1+\varphi_{\text{I}1}+\mu_{\text{H}})} + \frac{\chi_{\text{CM}}\sigma_{\text{CM}}S^*_{\text{CM}}}{N^*_{\text{H}}(\eta_2+\varphi_{\text{I}2}+\mu_{\text{H}})}\right)$$

3.2 Local asymptotic stability of the COVID-19 Free Equilibrium (CFE) of the co-infection model

Theorem 3.1 *The CFE, ξ_0, of the model* (1) *is locally asymptotically stable (LAS) if $\mathcal{R}_{0\text{C}} < 1$, and unstable if $\mathcal{R}_{0\text{C}} > 1$.*

Proof.
The local stability of the model (1) is analysed by the Jacobian matrix of the system (1) evaluated at the COVID-19-free equilibrium ξ_0, given by:

$$\begin{pmatrix} -\mu_{\text{H}} & 0 & -\frac{\beta_{\text{CV}}\mu_{\text{H}}}{\mu_{\text{H}}+\theta_{\text{CM}}} & 0 & 0 & -\frac{\beta_{\text{CV}}\mu_{\text{H}}\sigma_{\text{CM}}}{\mu_{\text{H}}+\theta_{\text{CM}}} & 0 & 0\\ \theta_{\text{CM}} & -\mu_{\text{H}} & -\frac{\beta_{\text{CV}}\chi_{\text{CM}}\theta_{\text{CM}}\sigma_{\text{CM}}}{\mu_{\text{H}}+\theta_{\text{CM}}} & 0 & 0 & -\frac{\beta_{\text{CV}}\chi_{\text{CM}}\theta_{\text{CM}}}{\mu_{\text{H}}+\theta_{\text{CM}}} & 0 & 0\\ 0 & 0 & \frac{\beta_{\text{CV}}\mu_{\text{H}}}{\mu_{\text{H}}+\theta_{\text{CM}}} - K_1 & 0 & 0 & \frac{\beta_{\text{CV}}\mu_{\text{H}}\sigma_{\text{CM}}}{\mu_{\text{H}}+\theta_{\text{CM}}} & 0 & 0\\ 0 & 0 & \eta_1 & -K_2 & 0 & 0 & 0 & 0\\ 0 & 0 & \varphi_{\text{I}1} & \varphi_{\text{Q}1} & -\mu_{\text{H}} & 0 & 0 & 0\\ 0 & 0 & \frac{\beta_{\text{CV}}\chi_{\text{CM}}\theta_{\text{CM}}}{\mu_{\text{H}}+\theta_{\text{CM}}} & 0 & 0 & \frac{\beta_{\text{CV}}\chi_{\text{CM}}\theta_{\text{CM}}\sigma_{\text{CM}}}{\mu_{\text{H}}+\theta_{\text{CM}}} - K_3 & 0 & 0\\ 0 & 0 & 0 & 0 & 0 & \eta_2 & -K_4 & 0\\ 0 & 0 & 0 & 0 & 0 & \varphi_{\text{I}2} & \varphi_{\text{Q}2} & -\mu_{\text{H}} \end{pmatrix}$$

where, $K_1 = \eta_1 + \varphi_{\text{I}1} + \mu_{\text{H}}, K_2 = \varphi_{\text{Q}1} + \delta_1 + \mu_{\text{H}}, K_3 = \eta_2 + \varphi_{\text{I}2} + \mu_{\text{H}}, K_4 = \varphi_{\text{Q}2} + \delta_1 + \delta_2 + \mu_{\text{H}}$.
The eigenvalues are given by $\lambda_1 = -(\eta_1 + \varphi_{\text{I}1} + \mu_{\text{H}})$, $\lambda_2 = -(\varphi_{\text{Q}1} + \delta_1 + \mu_{\text{H}})$, $\lambda_3 = -(\eta_2 + \varphi_{\text{I}2} + \mu_{\text{H}})$, $\lambda_4 = -(\varphi_{\text{Q}1} + \delta_1 + \delta_2 + \mu_{\text{H}})$ and the solutions of the characteristic polynomial

$$\lambda^2 + \left(K_1 + K_3 - \left(\frac{\beta_{\text{CV}}\mu_{\text{H}}}{\mu_{\text{H}}+\theta_{\text{CM}}} + \frac{\beta_{\text{CV}}\chi_{\text{CM}}\sigma_{\text{CM}}\theta_{\text{CM}}}{\mu_{\text{H}}+\theta_{\text{CM}}}\right)\right)\lambda + K_1K_3\left(1-\mathcal{R}_{0\text{C}}\right) = 0, \tag{4}$$

Applying the Routh-Hurwitz criterion, the quadratic equation (4) will have roots with negative real parts if and only if $\mathcal{R}_{0\text{C}} < 1$. As a result, the COVID-19-free equilibrium, ξ_0 is locally asymptotically stable if $\mathcal{R}_{0\text{C}} < 1$.
The epidemiological implication of Theorem 3.1 is that COVID-19 can be eliminated from the population when $\mathcal{R}_{0\text{C}} < 1$ and if the initial sizes of the population of the model are in the region of attraction of the CFE.

medRxiv preprint doi: https://doi.org/10.1101/2020.08.04.20168013; this version posted September 10, 2020. The copyright holder for this preprint (which was not certified by peer review) is the author/funder, who has granted medRxiv a license to display the preprint in perpetuity.
It is made available under a CC-BY-NC-ND 4.0 International license .

3.3 Existence of Endemic equilibrium points (EEP) of the model

In this section, we shall investigate the existence of an endemic equilibrium of the model (1). Let an arbitrary equilibrium point of the model be given by

$$\xi_e = \left(S_{\text{H}}^{**}, S_{\text{CM}}^{**}, I_{\text{CV}}^{**}, Q_{\text{CV}}^{**}, R_{\text{CV}}^{**}, I_{\text{CVCM}}^{**}, Q_{\text{CVCM}}^{**}, R_{\text{CM}}^{**}\right)$$

The steady state solutions of equations of the model (1)

$$\begin{aligned}
S_{\text{H}}^{**} &= \frac{\Lambda_{\text{H}}}{(\lambda_{\text{CV}}^{**} + \theta_{\text{CM}} + \mu_{\text{H}})}, \quad S_{\text{CM}}^{**} = \frac{\theta_{\text{CM}}\Lambda_{\text{H}}}{(\chi_{\text{CM}}\lambda_{\text{CV}}^{**} + \mu_{\text{H}})(\lambda_{\text{CV}}^{**} + \theta_{\text{CM}} + \mu_{\text{H}})},\\
I_{\text{CV}}^{**} &= \frac{\Lambda_{\text{H}}\lambda_{\text{CV}}^{**}(\mu_{\text{H}} + \psi_1\lambda_{\text{CV}}^{**})K_2}{(\lambda_{\text{CV}}^{**} + \theta_{\text{CM}} + \mu_{\text{H}})\left[K_1K_2\mu_{\text{H}} + (\mu_{\text{H}}\psi_1K_2 + \eta_1\psi_1(\delta_1 + \mu_{\text{H}}))\lambda_{\text{CV}}^{**}\right]},\\
Q_{\text{CV}}^{**} &= \frac{\Lambda_{\text{H}}\lambda_{\text{CV}}^{**}\eta_1(\mu_{\text{H}} + \psi_1\lambda_{\text{CV}}^{**})}{(\lambda_{\text{CV}}^{**} + \theta_{\text{CM}} + \mu_{\text{H}})\left[K_1K_2\mu_{\text{H}} + (\mu_{\text{H}}\psi_1K_2 + \eta_1\psi_1(\delta_1 + \mu_{\text{H}}))\lambda_{\text{CV}}^{**}\right]},\\
R_{\text{CV}}^{**} &= \frac{\Lambda_{\text{H}}\lambda_{\text{CV}}^{**}(\varphi_{\text{I1}}K_2 + \varphi_{\text{Q1}}\eta_1)}{(\lambda_{\text{CV}}^{**} + \theta_{\text{CM}} + \mu_{\text{H}})\left[K_1K_2\mu_{\text{H}} + (\mu_{\text{H}}\psi_1K_2 + \eta_1\psi_1(\delta_1 + \mu_{\text{H}}))\lambda_{\text{CV}}^{**}\right]},\\
I_{\text{CVCM}}^{**} &= \frac{\chi_{\text{CM}}\theta_{\text{CM}}\Lambda_{\text{H}}\lambda_{\text{CV}}^{**}(\mu_{\text{H}} + \psi_2\lambda_{\text{CV}}^{**})K_4}{(\lambda_{\text{CV}}^{**} + \theta_{\text{CM}} + \mu_{\text{H}})(\chi_{\text{CM}}\lambda_{\text{CV}}^{**} + \mu_{\text{H}})\left[K_3K_4\mu_{\text{H}} + (\mu_{\text{H}}\psi_2K_4 + \eta_2\psi_2(\delta_1 + \delta_2 + \mu_{\text{H}}))\lambda_{\text{CV}}^{**}\right]},\\
Q_{\text{CVCM}}^{**} &= \frac{\chi_{\text{CM}}\theta_{\text{CM}}\Lambda_{\text{H}}\lambda_{\text{CV}}^{**}\eta_2(\mu_{\text{H}} + \psi_2\lambda_{\text{CV}}^{**})}{(\lambda_{\text{CV}}^{**} + \theta_{\text{CM}} + \mu_{\text{H}})(\chi_{\text{CM}}\lambda_{\text{CV}}^{**} + \mu_{\text{H}})\left[K_3K_4\mu_{\text{H}} + (\mu_{\text{H}}\psi_2K_4 + \eta_2\psi_2(\delta_1 + \delta_2 + \mu_{\text{H}}))\lambda_{\text{CV}}^{**}\right]},\\
R_{\text{CVCM}}^{**} &= \frac{\chi_{\text{CM}}\theta_{\text{CM}}\Lambda_{\text{H}}\lambda_{\text{CV}}^{**}(\varphi_{\text{I2}}K_4 + \varphi_{\text{Q2}}\eta_2)}{(\lambda_{\text{CV}}^{**} + \theta_{\text{CM}} + \mu_{\text{H}})(\chi_{\text{CM}}\lambda_{\text{CV}}^{**} + \mu_{\text{H}})\left[K_3K_4\mu_{\text{H}} + (\mu_{\text{H}}\psi_2K_4 + \eta_2\psi_2(\delta_1 + \delta_2 + \mu_{\text{H}}))\lambda_{\text{CV}}^{**}\right]},
\end{aligned} \tag{5}$$

Substituting the above expressions into the force of infection, at steady state, gives the following polynomial

$$Q_1(\lambda_{\text{CV}}^{**})^4 + Q_2(\lambda_{\text{HM}}^{**})^3 + Q_3(\lambda_{\text{HM}}^{**})^2 + Q_4\lambda_{\text{HM}}^{**} + Q_5 = 0 \tag{6}$$

where

$$\begin{aligned}
Q_1 &= (\mu_{\text{H}}K_4\psi_2 + \eta_2\psi_2(\delta_1 + \delta_2 + \mu_{\text{H}}))(\psi_1\chi_{\text{CM}}K_2 + \psi_1\chi_{\text{D}}\eta_1) > 0,\\
Q_2 &= K_2K_4\mu_{\text{H}}^2\psi_1\psi_2 + K_2\mu_{\text{H}}\eta_2(\delta_1 + \delta_2 + \mu_{\text{H}})\psi_1\psi_2 + K_4\mu_{\text{H}}\eta_1(\delta_1 + \mu_{\text{H}})\psi_1\psi_2 + \eta_1\eta_2(\delta_1 + \mu_{\text{H}})(\delta_1 + \delta_2 + \mu_{\text{H}})\psi_1\psi_2\\
&\quad + K_3K_4\mu_{\text{H}}(\psi_1\chi_{\text{CM}}K_2 + \psi_1\chi_{\text{CM}}\eta_1) + (\mu_{\text{H}}\psi_2K_4 + \eta_2\psi_2(\delta_1 + \delta_2 + \mu_{\text{H}}))\big(\mu_{\text{H}}\psi_1K_2 + \mu_{\text{H}}\chi_{\text{CM}}K_2 + \mu_{\text{H}}\psi_1\eta_1 + \mu_{\text{H}}\chi_{\text{CM}}\eta_1\\
&\quad + \varphi_{\text{I1}}\chi_{\text{CM}}K_2 + \varphi_{\text{Q1}}\eta_1\chi_{\text{CM}}\big) + (\mu_{\text{H}}\psi_1K_2 + \eta_1\psi_1(\delta_1 + \mu_{\text{H}}))(\psi_2K_4 + \eta_2\psi_2)\theta_{\text{CM}}\chi_{\text{CM}} - \beta_{\text{CV}}\psi_1\chi_{\text{CM}}K_2\big(\mu_{\text{H}}\psi_2K_4\\
&\quad + \eta_2\psi_2(\delta_1 + \delta_2 + \mu_{\text{H}})\big),\\
Q_3 &= (\mu_{\text{H}} + \theta_{\text{CM}})K_2K_4\mu_{\text{H}}^2\psi_1\psi_2 + (\mu_{\text{H}} + \theta_{\text{CM}})\mu_{\text{H}}\eta_2K_2(\delta_1 + \delta_2 + \mu_{\text{H}})\psi_1\psi_2 + (\mu_{\text{H}} + \theta_{\text{CM}})\mu_{\text{H}}\eta_1K_4(\delta_1 + \mu_{\text{H}})\psi_1\psi_2\\
&\quad + (\mu_{\text{H}} + \theta_{\text{CM}})\eta_1\eta_2(\delta_1 + \mu_{\text{H}})(\delta_1 + \delta_2 + \mu_{\text{H}})\psi_1\psi_2 + \chi_{\text{CM}}\mu_{\text{H}}^2\psi_2K_1K_2K_4 + \chi_{\text{CM}}\mu_{\text{H}}\eta_2\psi_2(\delta_1 + \delta_2 + \mu_{\text{H}}) + \chi_{\text{CM}}\mu_{\text{H}}^2\psi_1K_2K_3K_4\\
&\quad + \chi_{\text{CM}}\mu_{\text{H}}\eta_1\psi_1K_3K_4(\delta_1 + \mu_{\text{H}}) + \mu_{\text{H}}^2(\psi_1 + \chi_{\text{CM}})K_2K_3K_4 + K_3K_4\mu_{\text{H}}^2\eta_1(\psi_1 + \chi_{\text{CM}}) + K_3K_4\chi_{\text{CM}}(K_2\varphi_{\text{I1}} + \mu_{\text{H}}\varphi_{\text{Q1}}\eta_1)\\
&\quad + (\mu_{\text{H}}\psi_2K_4 + \eta_2\psi_2(\delta_1 + \delta_2 + \mu_{\text{H}}))\left(\mu_{\text{H}}^2K_2K\mu_{\text{H}}^2\eta_1 + \mu_{\text{H}}\varphi_{\text{I1}}K_2 + \varphi_{\text{Q1}}\eta_1\mu_{\text{H}}\right) + \mu_{\text{H}}\psi_2K_1K_2\theta_{\text{CM}}\chi_{\text{CM}}(K_4 + \eta_2)\\
&\quad + (\mu_{\text{H}}\psi_1K_2 + \eta_1\psi_1\delta_1 + \eta_1\psi_1\mu_{\text{H}})(\theta_{\text{CM}}\chi_{\text{CM}}\mu_{\text{H}}K_4 + \theta_{\text{CM}}\chi_{\text{CM}}\eta_2\mu_{\text{H}} + \theta_{\text{CM}}\chi_{\text{CM}}\varphi_{\text{I2}}K_4\theta_{\text{CM}}\chi_{\text{CM}}\varphi_{\text{Q2}}\eta_2) - \beta_{\text{CV}}\psi_1\chi_{\text{CM}}\mu_{\text{H}}K_2K_3K_4\\
&\quad - \beta_{\text{CV}}\mu_{\text{H}}K_2(\chi_{\text{CM}} + \psi_1)(\mu_{\text{H}}\psi_2K_4 + \eta_2\psi_2(\delta_1 + \delta_2 + \mu_{\text{H}})) - \beta_{\text{CV}}\sigma_{\text{CM}}\theta_{\text{CM}}\psi_2K_4(\mu_{\text{H}}\psi_1K_2 + \eta_1\psi_1\chi_{\text{CM}}(\delta_1 + \mu_{\text{H}})),\\
Q_4 &= (\mu_{\text{H}} + \theta_{\text{CM}})\mu_{\text{H}}^2\psi_2K_1K_2K_4 + \mu_{\text{H}}\eta_2\psi_2K_1K_2(\mu_{\text{H}} + \theta_{\text{CM}})(\delta_1 + \delta_2 + \mu_{\text{H}}) + \mu_{\text{H}}^2\psi_1K_2K_3K_4(\mu_{\text{H}} + \theta_{\text{CM}}) + (\mu_{\text{H}} + \theta_{\text{CM}})\mu_{\text{H}}\eta_1\psi_1(\delta_1 + \mu_{\text{H}})\\
&\quad + \chi_{\text{CM}}\mu_{\text{H}}^2K_1K_2K_3K_4 + \mu_{\text{H}}K_3K_4\left(\mu_{\text{H}}^2K_2 + \mu_{\text{H}}^2\eta_1 + \varphi_{\text{I1}}\mu_{\text{H}}K_2 + \varphi_{\text{Q2}}\eta_1\mu_{\text{H}}\right) + \mu_{\text{H}}^2\chi_{\text{CM}}\theta_{\text{CM}}K_1K_2K_4 + \chi_{\text{CM}}\theta_{\text{CM}}\eta_2K_1K_2\\
&\quad + \mu_{\text{H}}\chi_{\text{CM}}\theta_{\text{CM}}\varphi_{\text{Q2}}\eta_2K_1K_2 - \beta_{\text{CV}}\mu_{\text{H}}^3\psi_1K_2K_4 - \beta_{\text{CV}}\mu_{\text{H}}^2\psi_2\eta_2K_2(\delta_1 + \delta_2 + \mu_{\text{H}}) - \beta_{\text{CV}}\mu_{\text{H}}^2K_2K_3K_4\chi_{\text{CM}}\\
&\quad - \beta_{\text{CV}}\mu_{\text{H}}^2\psi_1K_2K_3K_4 - \beta_{\text{CV}}\sigma_{\text{CM}}\chi_{\text{CM}}\theta_{\text{CM}}\mu_{\text{H}}K_4(\mu_{\text{H}}\psi_1K_2 + \eta_1\psi_1\delta_1 + \eta_1\psi_1\mu_{\text{H}})\\
&\quad - \beta_{\text{CV}}\sigma_{\text{CM}}\chi_{\text{CM}}\theta_{\text{CM}}\psi_2\mu_{\text{H}}K_1K_2K_4,\\
Q_5 &= (\mu_{\text{H}} + \theta_{\text{CM}})K_1K_2K_3K_4\mu_{\text{H}}^2(1 - \mathcal{R}_{0\text{C}})
\end{aligned} \tag{7}$$

The components of the EEP are obtained upon solving for λ_{CV}^{**} from the polynomial (6), and substituting the positive values of λ_{CV}^{**} into the expressions in (5). Moreover, it follows from (7) that the coefficient Q_1 is always positive, and Q_5 is positive (negative) if $\mathcal{R}_{0\text{C}}$ is less (greater) than one. The following results can be deduced.

Theorem 3.2 *The model* (1) *has:*

medRxiv preprint doi: https://doi.org/10.1101/2020.08.04.20168013; this version posted September 10, 2020. The copyright holder for this preprint (which was not certified by peer review) is the author/funder, who has granted medRxiv a license to display the preprint in perpetuity.
It is made available under a CC-BY-NC-ND 4.0 International license .

(i) four or two endemic equilibria if $Q_2 > 0, Q_3 < 0, Q_4 > 0$ *and* $\mathcal{R}_{0C} < 1$,

(ii) two endemic equilibria if $Q_2 > 0, Q_3 > 0, Q_4 < 0$ *and* $\mathcal{R}_{0C} < 1$

(ii) no endemic equilibrium otherwise, if $\mathcal{R}_{0C} < 1$,

The first two items of Theorem 3.2 ((i) - (ii)) suggest the possibility of backward bifurcation in the model (1) when $\mathcal{R}_{0C} < 1$. It is worthy of note to show that, setting the parameters $\psi_1 = \psi_2 = \chi_{CM} = 0$, reduces the quartic (6) to $\mu_H K_3 K_4 \left(\mu_H^2 K_2 + \mu_H^2 \eta_1 + \varphi_{I1}\mu_H K_2 + \varphi_{Q2}\eta_1\mu_H\right)\lambda_{CV}^{**} + (\mu_H + \theta_{CM})K_1K_2K_3K_4\mu_H^2(1 - \mathcal{R}_{0C}) = 0$, resulting in no sign changes in the polynomial equation for $\mathcal{R}_{0C} < 1$. However, for $\mathcal{R}_{0C} < 1$ a unique endemic equilibrium exists. In the subsequent section, we shall explore the existence of the phenomenon of backward bifurcation in the model (1).

3.4 Backward bifurcation analysis of the model (1)

In this section, we shall seek to determine the type of bifurcation the model (1) will exhibit, using the Center Manifold theory presented by Castillo-Chavez and Song [8]. We establish the result below

Theorem 3.3 *Suppose a backward bifurcation coefficient* $a > 0$, *(with a defined below), when* $\mathcal{R}_0 < 1$

$$a = -\frac{2\beta_{CV}^*(x_1^*\nu_3 + x_2^*\nu_6)}{N_H^{*2}}(\omega_3 + \sigma_{CM}\omega_6)(\omega_1 + \omega_2 + \omega_3 + \omega_4\omega_5 + \omega_6 + \omega_7 + \omega_8)$$
$$+ \frac{2\beta_{CV}^*(\omega_3 + \sigma_{CM}\omega_6)}{N_H^*}\left((\omega_1 + \psi_1\omega_5)\nu_3 + (\omega_2 + \psi_2\omega_8)\nu_6\right)$$

then model (1) *undergoes the phenomenon of backward bifurcation at* $\mathcal{R}_{0C} = 1$. *If* $a < 0$, *then the system* (1) *exhibits a forward bifurcation at* $\mathcal{R}_{0C} = 1$.

Proof
Suppose

$$\xi_e = (S_H^{**}, S_{CM}^{**}, I_{CV}^{**}, Q_{CV}^{**}, R_{CV}^{**}, I_{CVCM}^{**}, Q_{CVCM}^{**}, R_{CM}^{**})$$

represents any arbitrary endemic equilibrium of the model. To apply the Center Manifold theory, it is important we carry out the change of variables below.
Let

$$S_H = x_1, S_{CM} = x_2, I_{CV} = x_3, Q_{CV} = x_4, R_{CV} = x_5, I_{CVCM} = x_6, Q_{CVCM} = x_7, R_{CM} = x_8$$

Moreover, using the vector notation

$$X = (x_1, x_2, x_3, x_4, x_5, x_6, x_7, x_8)^T$$

the model (1) can be re-written in the form

$$\frac{dX}{dt} = f = (f_1, f_2, f_3, f_4, f_5, f_6, f_7, f_8)^T$$

as follows:

$$\begin{aligned}
\frac{dx_1}{dt} &= \Lambda_H - (\lambda_{CV} + \theta_{CM} + \mu_H)x_1 \\
\frac{dx_2}{dt} &= \theta_{CM}x_1 - \chi_{CM}\lambda_{CV}x_2 - \mu_H x_2 \\
\frac{dx_3}{dt} &= \lambda_{CV}x_1 - (\eta_1 + \varphi_{I1} + \mu_H)x_3 + \psi_1\lambda_{CV}x_5 \\
\frac{dx_4}{dt} &= \eta_1 x_3 - (\varphi_{Q1} + \delta_1 + \mu_H)x_4 \\
\frac{dx_5}{dt} &= \varphi_{I1}x_3 + \varphi_{Q1}x_4 - \mu_H x_5 - \psi_1\lambda_{CV}x_5 \\
\frac{dx_6}{dt} &= \chi_{CM}\lambda_{CV}x_2 - (\eta_2 + \varphi_{I2} + \mu_H)x_6 + \psi_2\lambda_{CV}x_8 \\
\frac{dx_7}{dt} &= \eta_2 x_6 - (\delta_1 + \delta_2 + \varphi_{Q2} + \mu_H)x_7 \\
\frac{dx_8}{dt} &= \varphi_{I2}x_6 + \varphi_{Q2}x_7 - \mu_H x_8 - \psi_2\lambda_{CV}x_8
\end{aligned} \tag{8}$$

medRxiv preprint doi: https://doi.org/10.1101/2020.08.04.20168013; this version posted September 10, 2020. The copyright holder for this preprint (which was not certified by peer review) is the author/funder, who has granted medRxiv a license to display the preprint in perpetuity.
It is made available under a CC-BY-NC-ND 4.0 International license .

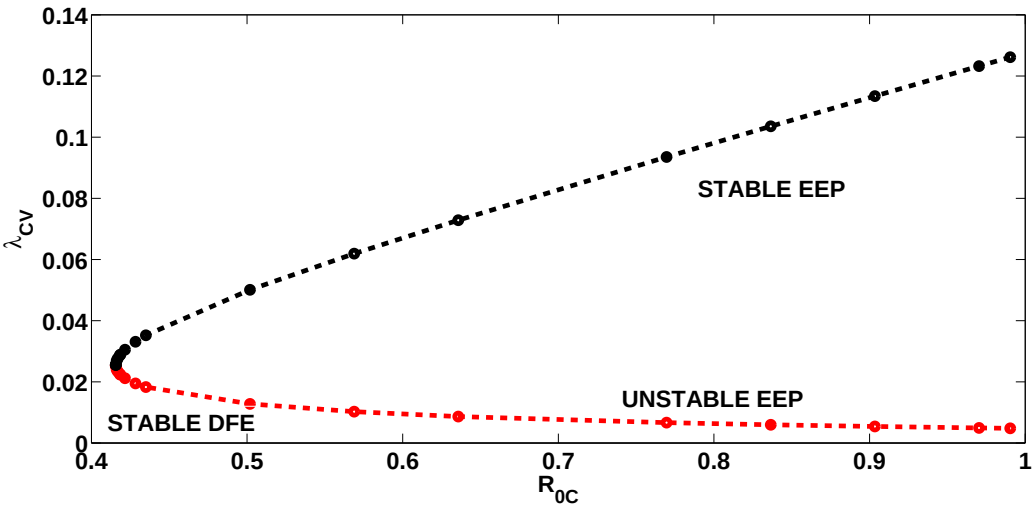

Figure 2: Bifurcation diagram for the model (1). Parameter values used are: $\beta_{\text{CV}} = 0.148, \psi_1 = 25, \psi_2 = 40, \chi_{\text{CM}} = 1.2$. All other parameters as in Table 1

with

$$\lambda_{\text{CV}} = \frac{\beta_{\text{CV}}(x_3 + \sigma_{\text{CM}} x_6)}{\sum_{i=1}^{8} x_i},$$

Consider the case when $\mathcal{R}_{0\text{C}} = 1$. Moreover, let β_{CV} be chosen as a bifurcation parameter. Solving for $\beta_{\text{CV}} = \beta^*_{\text{CV}}$ from $\mathcal{R}_{0\text{C}} = 1$ we obtain

$$\beta_{\text{CV}} = \beta^*_{\text{CV}} = \frac{K_1 K_3(\mu_{\text{H}} + \theta_{\text{CM}})}{(\mu_{\text{H}} K_3 + \chi_{\text{CM}}\sigma_{\text{CM}}\theta_{\text{CM}} K_1)}$$

Evaluating the Jacobian of the system (1) at the CFE, $J(\xi_0)$, and evaluating the right eigenvector, $\mathbf{w} = [\omega_1, \omega_2, \omega_3, \omega_4, \omega_5, \omega_6, \omega_7, \omega_8]^T$, associated with the simple zero eigenvalue of $J(\xi_0)$, gives

$$\omega_1 = -\frac{K_1 K_3 \Lambda_{\text{H}}(\omega_3 + \omega_6)}{(\mu_{\text{H}} K_3 + \chi_{\text{CM}}\sigma_{\text{CM}}\theta_{\text{CM}} K_1)} < 0, \quad \omega_2 = \frac{K_1 K_3 \theta_{\text{CM}}(\Lambda_{\text{H}} + \chi_{\text{CM}})(\omega_3 + \omega_6)}{(\mu_{\text{H}} K_3 + \chi_{\text{CM}}\sigma_{\text{CM}}\theta_{\text{CM}} K_1)} > 0, \quad \omega_3 = \omega_3 > 0,$$
$$\omega_4 = \frac{\eta_1 \omega_3}{K_2} > 0,, \quad \omega_5 = \frac{(\varphi_{\text{I1}} K_2 + \varphi_{\text{Q1}}\eta_1)\omega_3}{\mu_{\text{H}} K_2} > 0, \quad \omega_6 = \omega_6 > 0, \quad \omega_7 = \frac{\eta_2 \omega_6}{K_4} > 0, \quad \omega_8 = \frac{(\varphi_{\text{I2}} K_4 + \varphi_{\text{Q2}}\eta_2)\omega_6}{\mu_{\text{H}} K_4} > 0 \tag{9}$$

Likewise, the components of the left eigenvector of $J(\xi_0)|_{\beta_{\text{CV}}=\beta^*_{\text{CV}}}$, $\mathbf{v} = (\nu_1, \nu_2, ..., \nu_8)$, satisfying $\mathbf{v}.\mathbf{w} = 1$ are

$$\nu_1 = \nu_2 = 0, \quad \nu_3 = \nu_3 > 0, \quad \nu_4 = \nu_5 = 0, \quad \nu_6 = \nu_6 > 0, \quad \nu_7 = \nu_8 = 0 \tag{10}$$

The associated bifurcation coefficients defined by a and b, given by:

$$a = \sum_{k,i,j=1}^{n} \nu_k \omega_i \omega_j \frac{\partial^2 f_k}{\partial x_i \partial x_j}(0,0) \quad \text{and} \quad b = \sum_{k,i=1}^{n} \nu_k \omega_i \frac{\partial^2 f_k}{\partial x_i \partial \beta^*_{\text{CV}}}(0,0),$$

are computed to be

$$\begin{aligned} a = &-\frac{2\beta^*_{\text{CV}}(x_1^* \nu_3 + x_2^* \nu_6)}{N_{\text{H}}^{*2}}(\omega_3 + \sigma_{\text{CM}}\omega_6)(\omega_1 + \omega_2 + \omega_3 + \omega_4\omega_5 + \omega_6 + \omega_7 + \omega_8) \\ &+ \frac{2\beta^*_{\text{CV}}(\omega_3 + \sigma_{\text{CM}}\omega_6)}{N^*}\left((\omega_1 + \psi_1\omega_5)\nu_3 + (\omega_2 + \psi_2\omega_8)\nu_6\right) \end{aligned} \tag{11}$$

and

$$b = \sum_{k,i=1}^{20} \nu_k \omega_i \frac{\partial^2 f_k}{\partial x_i \partial \beta^*_{\text{CV}}}(0,0) = \frac{(\omega_3 + \sigma_{\text{CM}}\omega_6)}{\mu_{\text{H}} + \theta_{\text{CM}}}(\mu_{\text{H}}\nu_3 + \theta_{\text{CM}}\nu_6) > 0$$

medRxiv preprint doi: https://doi.org/10.1101/2020.08.04.20168013; this version posted September 10, 2020. The copyright holder for this preprint (which was not certified by peer review) is the author/funder, who has granted medRxiv a license to display the preprint in perpetuity.
It is made available under a CC-BY-NC-ND 4.0 International license .

It is observed that the bifurcation coefficient b is positive. Hence, following from Theorem 4.1 in [8] we have that the model (1) exhibits backward bifurcation phenomenon if the backward bifurcation coefficient, a, given by (11) is positive. The associated backward bifurcation diagram is presented in Figure 2. It is imperative to note, that setting the COVID-19 re-infection terms $\psi_1 = \psi_2 = 0$ as well as the modification parameter for increased susceptibility to COVID-19 by comorbid susceptibles $\chi_{\text{CM}} = 0$, we observed that the bifurcation coefficient, $a < 0$. As a result, backward bifurcation does not occur in the COVID-19-comorbidity co-infection model, when there is no re-infection after recovery from COVID-19 and when appropriate measures are enforced to prevent comorbid susceptible individuals from getting infected with COVID-19. This result is consistent with the result obtained in Section 3.3 above. The epidemiological interpretation is that if this phenomenon occurs, then the control of COVID-19 at the community level becomes difficult, even when the associated reproduction number $\mathcal{R}_{0\text{C}} < 1$.

3.5 Global asymptotic stability of the CFE of the model

By removing the cause of the backward bifurcation in the model (1), that is, setting $\psi_1 = \psi_2 = \chi_{\text{CM}} = 0$, we have the following reduced model.

$$\begin{aligned}
\frac{dS_{\text{H}}}{dt} &= \Lambda_{\text{H}} - (\lambda_{\text{CV}} + \theta_{\text{CM}} + \mu_{\text{H}})S_{\text{H}} \\
\frac{dS_{\text{CM}}}{dt} &= \theta_{\text{CM}}S_{\text{H}} - \mu_{\text{H}}S_{\text{CM}} \\
\frac{dI_{\text{CV}}}{dt} &= \lambda_{\text{CV}}S_{\text{H}} - K_1 I_{\text{CV}} \\
\frac{dQ_{\text{CV}}}{dt} &= \eta_1 I_{\text{CV}} - K_2 Q_{\text{CV}} \\
\frac{dR_{\text{CV}}}{dt} &= \varphi_{\text{I1}} I_{\text{CV}} + \varphi_{\text{Q1}} Q_{\text{CV}} - \mu_{\text{H}} R_{\text{CV}}
\end{aligned} \tag{12}$$

with

$$\lambda_{\text{CV}} = \frac{\beta_{\text{CV}} I_{\text{CV}}}{N_{\text{H}}},$$

We can prove the global asymptotic stability of the CFE of the model (1).

Theorem 3.4 *Consider the model* (1) *with* $\psi_1 = \psi_2 = \chi_{\text{CM}} = 0$. *The CFE is GAS in* $\mathcal{D}$ *whenever* $\bar{\mathcal{R}}_{0\text{C}} = \mathcal{R}_{0\text{C}}|_{\chi_{\text{CM}}=0} \leq 1$

Proof. We notice the compartments S_{CM}, Q_{CV} and R_{CV}, do not impact the dynamics of COVID-19 in the considered epidemic model. Therefore, we continue our proof with the compartments S_{H}, and I_{CV}. For the rest of the proof, we consider the following Lyapunov function

$$\mathcal{L} = S_{\text{H}} - S_{\text{H}}^* - S_{\text{H}}^* \ln\left(\frac{S_{\text{H}}}{S_{\text{H}}^*}\right) + \frac{1}{2} I_{\text{CV}}^2 \tag{13}$$

Applying the derivative of the Lyapunov function (13) along the trajectories of the considered model, we have the following relationships

$$\begin{aligned}
\dot{\mathcal{L}} &= \left(1 - \frac{S_{\text{H}}^*}{S_{\text{H}}}\right)\frac{dS_{\text{H}}}{dt} + I_{\text{CV}}\frac{dI_{\text{CV}}}{dt}, \\
&= \left(1 - \frac{S_{\text{H}}^*}{S_{\text{H}}}\right)\left[\Lambda_{\text{H}} - (\lambda_{\text{CV}} + \theta_{\text{CM}} + \mu_{\text{H}})\, S_{\text{H}}\right] + I_{\text{CV}}\left[\lambda_{\text{CV}}S_{\text{H}} - K_1 I_{\text{CV}}\right], \\
&= \left(1 - \frac{S_{\text{H}}^*}{S_{\text{H}}}\right)\left[\Lambda_{\text{H}} - (\lambda_{\text{CV}} + \theta_{\text{CM}} + \mu_{\text{H}})\, S_{\text{H}}\right] + I_{\text{CV}}^2\left[\frac{\beta_{\text{CV}}S_{\text{H}}}{N_{\text{H}}} - K_1\right],
\end{aligned} \tag{14}$$

At the COVID-19 free equilibrium point (CFE), we have the following form

$$\begin{aligned}
\dot{\mathcal{L}} &= -(\lambda_{\text{CV}} + \theta_{\text{CM}} + \mu_{\text{H}})\frac{(S_{\text{H}} - S_{\text{H}}^*)^2}{S_{\text{H}}} + I_{\text{CV}}^2\left[\frac{\beta_{\text{CV}}S_{\text{H}}^*}{N_{\text{H}}^*} - K_1\right], \\
&\leq -(\lambda_{\text{CV}} + \theta_{\text{CM}} + \mu_{\text{H}})\frac{(S_{\text{H}} - S_{\text{H}}^*)^2}{S_{\text{H}}} + \frac{I_{\text{CV}}^2}{K_1}\left(\bar{\mathcal{R}}_{0\text{C}} - 1\right)
\end{aligned} \tag{15}$$

medRxiv preprint doi: https://doi.org/10.1101/2020.08.04.20168013; this version posted September 10, 2020. The copyright holder for this preprint (which was not certified by peer review) is the author/funder, who has granted medRxiv a license to display the preprint in perpetuity.
It is made available under a CC-BY-NC-ND 4.0 International license .

Hence, $\mathcal{L} < 0$ if and only if $\bar{\mathcal{R}}_{0\text{C}} \leq 1$. Therefore, $\mathcal{L}$ is a Lyapunov function for the system (12). It follows by the La Salle's Invariance Principle [24], that the CFE of the model (12) is globally asymptotically stable whenever $\bar{\mathcal{R}}_{0\text{C}} \leq 1$.

4 Numerical simulations

4.1 Uncertainty and sensitivity analyses

As a result of the uncertainties which are expected to come up in parameter estimates used in the numerical simulations, a Latin Hypercube Sampling (LHS) [3] is implemented on the parameters of the model. For the sensitivity analysis, we carry out a Partial Rank Correlation Coefficient (PRCC) between values of the parameters in the response function and the values of the response function derived from the sensitivity analysis. 1,000 simulations of the co-infection model (1) *per* LHS were run. Using the reproduction number, $\mathcal{R}_{0\text{C}}$, as the response function, we observed in Table 2 that the top-ranked parameters that drive the dynamics of the co-infection model are the effective contact rate for COVID-19 transmission, β_{CV}, the parameter accounting for increased for susceptibility to COVID-19 by comorbid susceptible individuals, χ_{CM}, the parameter accounting for the infectiousness of co-infected individuals, σ_{CM}, the detection rates for singly infected and co-infected individuals, η_1 and η_2, respectively. Also, when the total number of individuals singly infected with COVID-19, I_{CV}, is used as the response function, the top ranked parametrs that influnce the dynamics of COVID-19 disease are the effective contact rate for COVID-19 transmission, β_{CV}, the parameter accounting for increased for the infectiousness of co-infected individuals, σ_{CM}, the detection rates for singly infected and co-infected individuals, η_1 and η_2, as well as the recovery rate from COVID-19, φ_{I1}.

Using the total number of isolated/hospitalized individuals with COVID-19, (Q_{CV}), as the response function, the parameters that strongly determine the dynamics of the model (1) are the effective contact rate for COVID-19 transmission, β_{CV}, the parameter accounting for increased for the infectiousness of co-infected individuals, σ_{CM}, the detection rates for singly infected and co-infected individuals, η_1 and η_2, as well as the recovery rates from COVID-19, φ_{I1} and φ_{Q1} for individuals in compartments I_{CV} and Q_{CV}, respectively. In addition, when the population of individuals co-infected with COVID-19 and comorbidity is used as response function, the top ranked parameters that drive the dynamics of the co-infection model are the effective contact rate for COVID-19 transmission, β_{CV}, the parameter accounting for increased sucseptibility to COVID-19 by comorbid susceptibles, χ_{CM}, the comorbidity development rate, θ_{CM}, the detection rate for singly infected and co-infected individuals, η_1 and η_2, as well as the recovery rate from COVID-19 for co-infected individuals, φ_{I2}. Moreover, when the population of isolated/hospitalized individuals with COVID-19 and comorbidity Q_{CVCM}, is used as response function, the parameters that drive the dynamics of the co-infection model are the effective contact rate for COVID-19 transmission, β_{CV}, the parameter accounting for increased sucseptibility to COVID-19 by comorbid susceptibles, χ_{CM}, the comorbidity development rate, θ_{CM}, the detection rates for co-infected individuals, η_2, as well as the recovery rates from COVID-19, φ_{I2} and φ_{Q2} for individuals in compartments I_{CV} and Q_{CV}, respectively.

4.2 Model Fitting and estimation of parameters and initial conditions

The population of Lagos is approximately estimated at 14,368,332 [45]. Also, based on a study carried out by Dahiru *et al.* [15] on the prevalence of diabetes mellitus in Lagos, Nigeria and since the first COVID-19 case in Lagos (with no evidence of comorbidity) was announced on March 16, 2020, we set our initial conditions to be $S_{\text{H}}(0) = 0.93 \times 14368332, S_{\text{CM}}(0) = 0.07 \times 14368332, Q_{\text{CV}}(0) = 1, R_{\text{CV}}(0) = 0, Q_{\text{CVCM}} = 0, R_{\text{CM}}(0) = 0$.

Two optimization algorithms were combined for data fitting, a genetic algorithm (GA) algorithm and the *fmincon* algorithm [27, 32] in MATLAB to estimate the values of the effective contact rate for COVID-19 transmission, β_{CV}, the case detection rates for singly infected and co-infected individuals, η_1 and η_2, respectively, the comorbidity induced death rate for co-infected individuals, δ_2 and the COVID-19 re-infection rates ψ_1 and ψ_2 for singly and co-infected individuals respectively. We equally estimated the initial conditions $I_{\text{CV}}(0)$ and $I_{\text{CVCM}}(0)$. All the estimates were done using the daily confirmed and active cases for Lagos, Nigeria, from March 16, 2020 to June 24, 2020 [29]. Table 3 gives the estimated values of $\beta_{\text{CV}}, \eta_1, \eta_2, \delta_2, \psi_1$ and ψ_2, and the initial conditions $I_{\text{CV}}(0)$ and $I_{\text{CVCM}}(0)$, together with the calculated

medRxiv preprint doi: https://doi.org/10.1101/2020.08.04.20168013; this version posted September 10, 2020. The copyright holder for this preprint (which was not certified by peer review) is the author/funder, who has granted medRxiv a license to display the preprint in perpetuity.
It is made available under a CC-BY-NC-ND 4.0 International license .

Table 2: PRCC values for the co-infection model (1) parameters using the total number of infected individuals and the reproduction number $\mathcal{R}_{0C}$ as response functions.

Parameters	I_{CV}	Q_{CV}	I_{CVCM}	Q_{CVCM}	$\mathcal{R}_{0C}$
μ_H	-0.0856	-0.0287	-0.0153	-0.0212	-0.0085
β_{CV}	**0.9800**	**0.9649**	**0.8857**	**0.7429**	**0.9348**
χ_{CM}	0.2080	0.1715	**0.5413**	**0.4001**	**0.6883**
θ_{CM}	0.0989	0.1022	**0.4531**	**0.4031**	-0.0027
σ_{CM}	**0.6956**	**0.6280**	0.3828	0.2436	**0.6079**
η_1	**-0.9456**	**0.6872**	**-0.5373**	-0.3472	**-0.6444**
η_2	**-0.6434**	**-0.5263**	**-0.9000**	**0.7933**	**-0.7336**
φ_{I1}	**-0.6817**	**-0.5669**	-0.2234	-0.0913	-0.2770
φ_{I2}	-0.2951	0.2156	**-0.5231**	**-0.4052**	-0.3436
φ_{Q1}	0.0112	**-0.7534**	-0.0309	0.0457	–
φ_{Q2}	0.0173	0.0393	0.0738	**-0.9090**	–
δ_1	0.0346	-0.2450	0.0087	-0.3801	–
δ_2	0.0110	-0.0187	0.0119	-0.3830	–
ψ_1	-0.0065	0.0512	-0.0839	-0.0315	–
ψ_2	0.0184	0.0034	0.0522	0.0365	–

reproduction number (R_{0C}).

Parameter	**Baseline value**	**Range**	**Reference**
μ_H	0.0000491 /day		[26]
Λ_H	705 /day		[45, 26]
β_{CV}	0.2001	[0.1, 0.3]	Fitted
$\varphi_{I1}, \varphi_{I2}$	0.13978 /day	$[\frac{1}{30}, \frac{1}{3}]$/day	[42]
φ_{Q1}, φ_{Q1}	$\frac{1}{15}$ /day	$[\frac{1}{30}, \frac{1}{3}]$/day	estimated from [9]
δ_1	0.015 /day	$[0.001, 0.1]$	[16]
η_1	0.0059 /day	[0.001,0.05]	Fitted
η_2	0.0895 /day	[0.001,0.05]	Fitted
θ_{CM}	0.0000034294	[0.0000001,0.00001]	Fitted
ψ_1	0.0013	[0.001,0.005]	Fitted
ψ_2	0.0013	[0.001,0.005]	Fitted
χ_{CM}	1.2	[1,3]	Inferred from [10]
σ_{CM}	1.2	[1,3]	Assumed
δ_2	0.0500	[0.01,0.08]	Fitted
$I_{CV}(0)$	135	[100,400]	Fitted
$I_{CVCM}(0)$	21	[20,50]	Fitted
$\mathcal{R}_{0C}$	1.3423		

Table 3: Estimated parameters and variables when the model 1 was fitted using the cumulative number of confirmed and active cases. The estimates were from the "best fit".

4.3 Discussion of results

Figure 3 presents the fitting of the model when the cumulative active cases were used to fit the model. The figure showed that the co-infection model (1) fitted well to the Lagos COVID-19 data (daily cumulative active cases).

As observed in Figure 4, the projection is made for the cumulative number of active cases using the developed model. It is observed that the cumulative active cases (including those with comorbidity) peaked at 130,000 cases in about 180 days (counting from March 16, 2020). Figure 5 presents the simulations of the cumulative number of active cases (including those with comorbidity) at different levels of susceptibility of comorbid susceptibles ($0.2 \leq \chi_{CM} \leq 1.2$). It is observed that the peak value attained at different

medRxiv preprint doi: https://doi.org/10.1101/2020.08.04.20168013; this version posted September 10, 2020. The copyright holder for this preprint **(which was not certified by peer review)** is the author/funder, who has granted medRxiv a license to display the preprint in perpetuity.
It is made available under a CC-BY-NC-ND 4.0 International license .

levels and reduces with decreasing value of the modification parameter χ_{CM}. We notice that as preventive measures such as social distancing, use of face mask in public places are enforced to reduce the probability of infection by comorbid susceptibles, the infection peaks reduce stedily. Similar conclusions are reached when the cumulative number of active cases (without comorbidity) are simulated, as seen in Figure 6. The simulations of the cumulative number of active cases (including those with comorbidity), at different re-infection rates, depicted in Figure 7 shows the attainment of infections peaks around 200 days (counting from March 16, 2020), although infection peak reduces with decreasing re-infection of those who have recovered from a previous COVID-19 infection. Figure 8 is interpreted in a similar manner. It is also observed that, when the cumulative number of active cases are sumulated at different infectivity rates for co-infected individuals, the infecton curves behave in a similar trend, as when the modification parameter χ_{CM} are varied (See Figures 9 and 10).

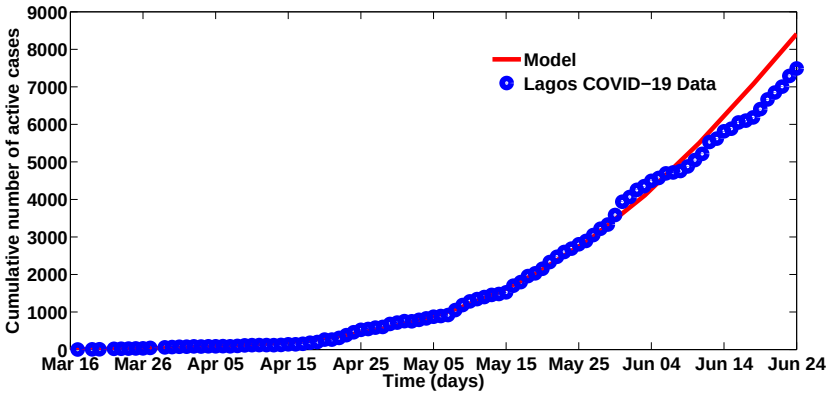

Figure 3: Fitting the cumulative number of active cases

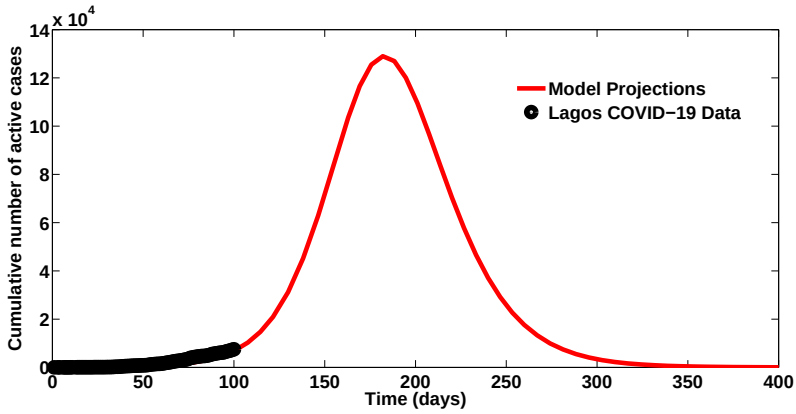

Figure 4: Projections for the cumulative number of active cases

medRxiv preprint doi: https://doi.org/10.1101/2020.08.04.20168013; this version posted September 10, 2020. The copyright holder for this preprint **(which was not certified by peer review)** is the author/funder, who has granted medRxiv a license to display the preprint in perpetuity.
It is made available under a CC-BY-NC-ND 4.0 International license .

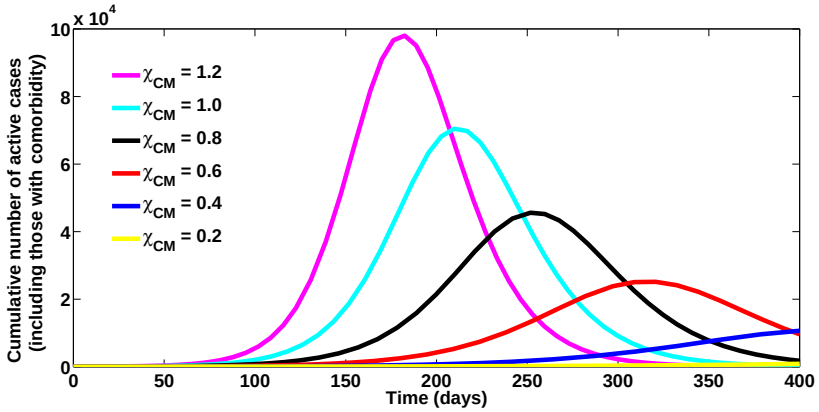

Figure 5: Simulations of the Cumulative number of active cases (including those with comorbidity): effect of χ_{CM}

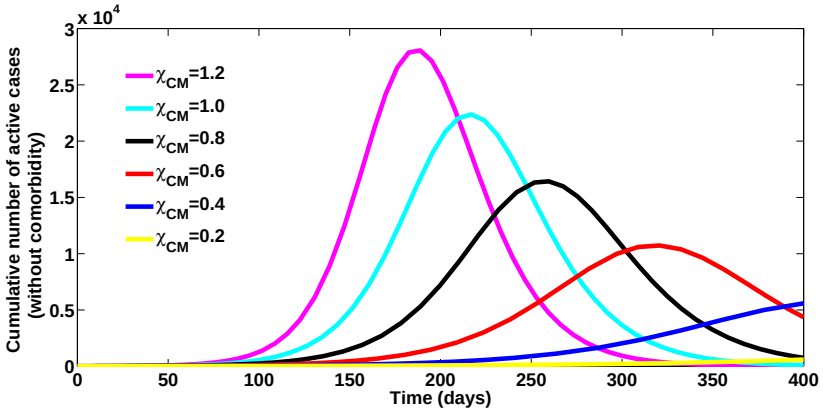

Figure 6: Simulations of the Cumulative number of active cases (without comorbidity): effect of χ_{CM}

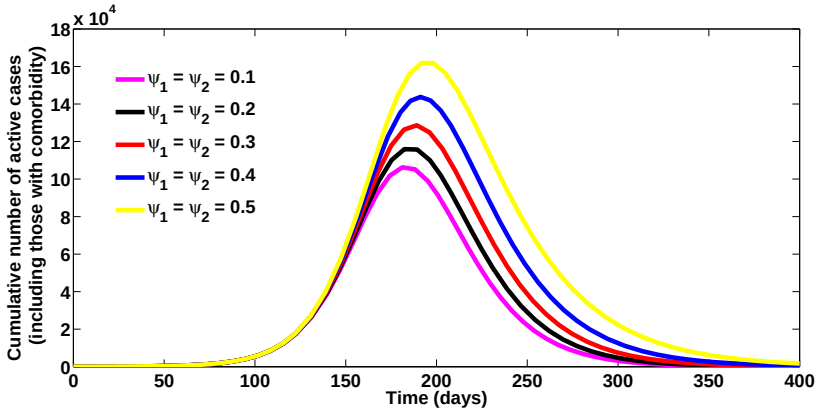

Figure 7: Simulations of the Cumulative number of active cases (including those with comorbidity): effect of ψ_1 and ψ_2

medRxiv preprint doi: https://doi.org/10.1101/2020.08.04.20168013; this version posted September 10, 2020. The copyright holder for this preprint **(which was not certified by peer review)** is the author/funder, who has granted medRxiv a license to display the preprint in perpetuity.
It is made available under a CC-BY-NC-ND 4.0 International license .

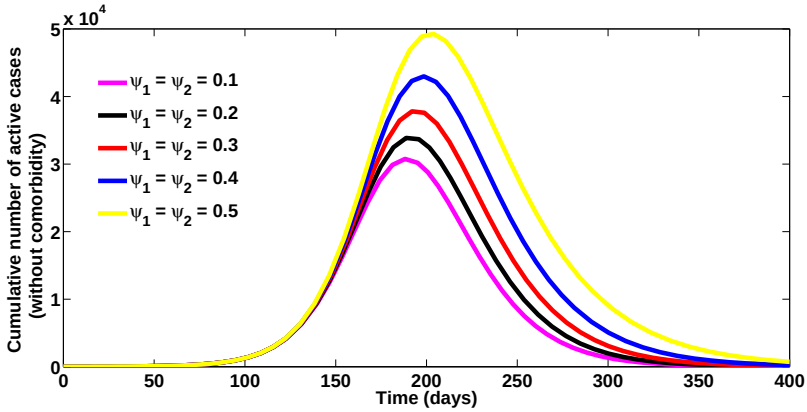

Figure 8: Simulations of the Cumulative number of active cases (without comorbidity): effect of ψ_1 and ψ_2

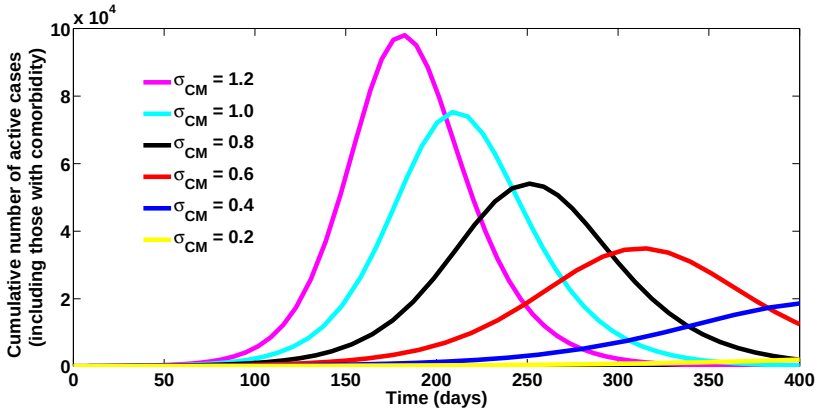

Figure 9: Simulations of the Cumulative number of active cases (including those with comorbidity): effect of σ_{CM}

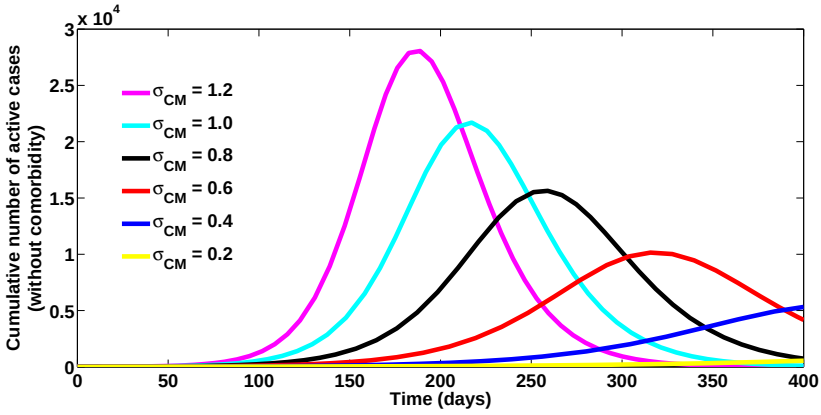

Figure 10: Simulations of the Cumulative number of active cases (without comorbidity): effect of σ_{CM}

medRxiv preprint doi: https://doi.org/10.1101/2020.08.04.20168013; this version posted September 10, 2020. The copyright holder for this preprint **(which was not certified by peer review)** is the author/funder, who has granted medRxiv a license to display the preprint in perpetuity.
It is made available under a CC-BY-NC-ND 4.0 International license .

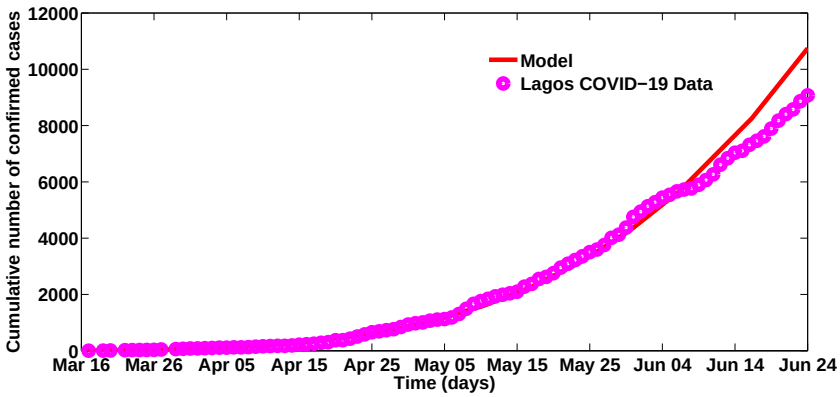

Figure 11: Fitting the cumulative number of confirmed cases

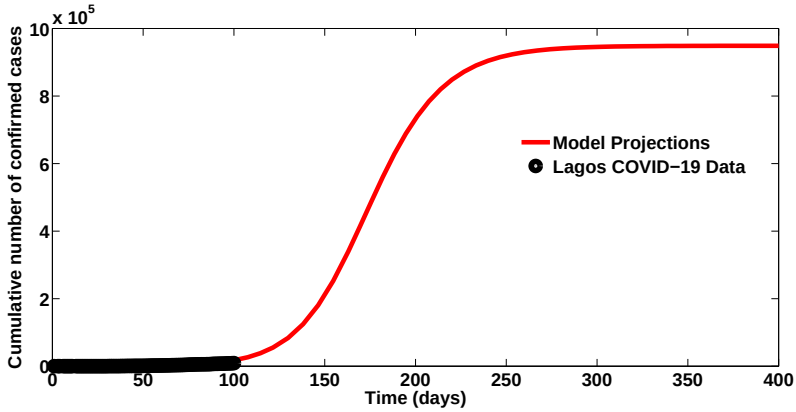

Figure 12: Projections for the cumulative number of confirmed cases

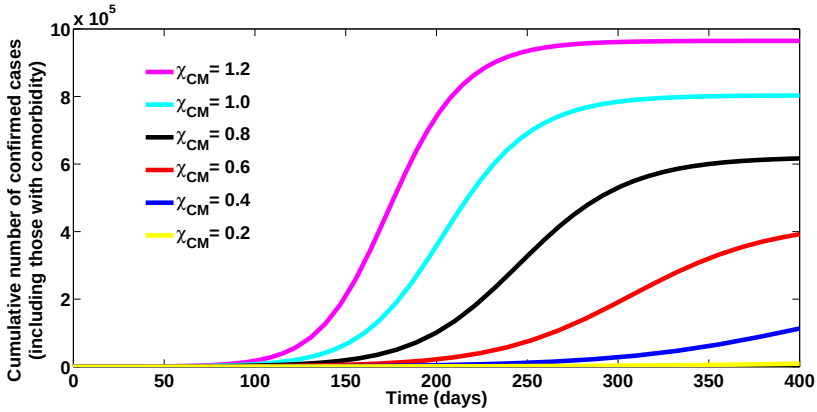

Figure 13: Simulations of the Cumulative number of confirmed cases (including those with comorbidity): effect of χ_{CM}

medRxiv preprint doi: https://doi.org/10.1101/2020.08.04.20168013; this version posted September 10, 2020. The copyright holder for this preprint **(which was not certified by peer review)** is the author/funder, who has granted medRxiv a license to display the preprint in perpetuity.
It is made available under a CC-BY-NC-ND 4.0 International license .

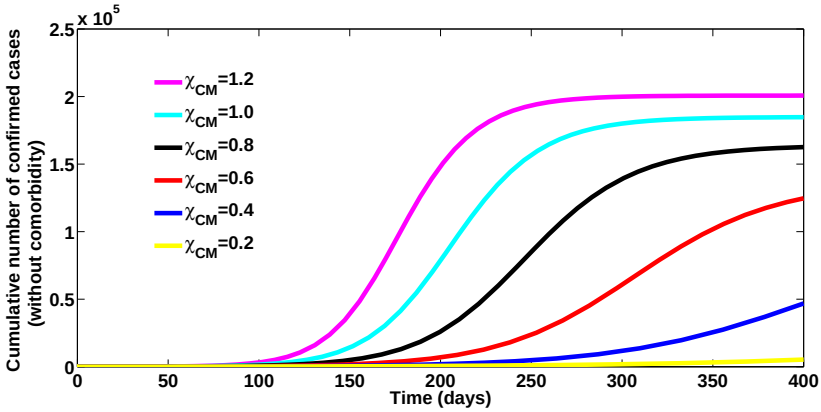

Figure 14: Simulations of the Cumulative number of confirmed cases (without comorbidity): effect of χ_{CM}

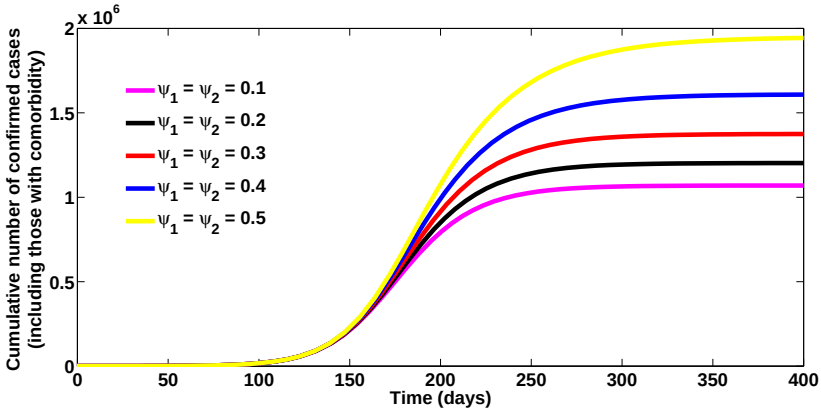

Figure 15: Simulations of the Cumulative number of confirmed cases (including those with comorbidity): effect of ψ_1 and ψ_2

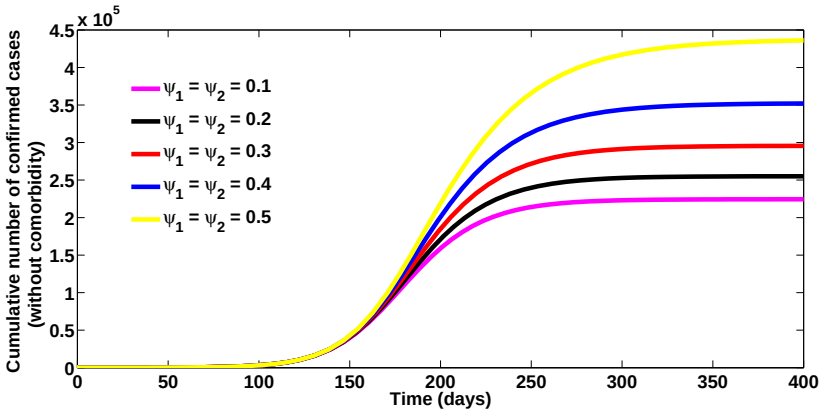

Figure 16: Simulations of the Cumulative number of confirmed cases (without comorbidity): effect of ψ_1 and ψ_2

medRxiv preprint doi: https://doi.org/10.1101/2020.08.04.20168013; this version posted September 10, 2020. The copyright holder for this preprint **(which was not certified by peer review)** is the author/funder, who has granted medRxiv a license to display the preprint in perpetuity.
It is made available under a CC-BY-NC-ND 4.0 International license .

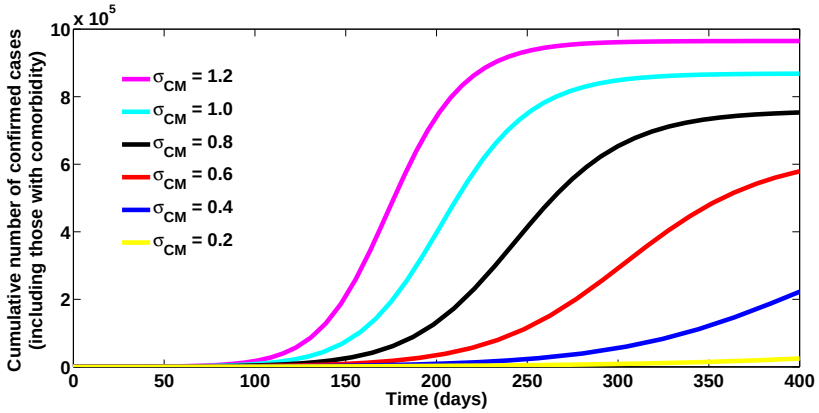

Figure 17: Simulations of the Cumulative number of confirmed cases (including those with comorbidity): effect of σ_{CM}

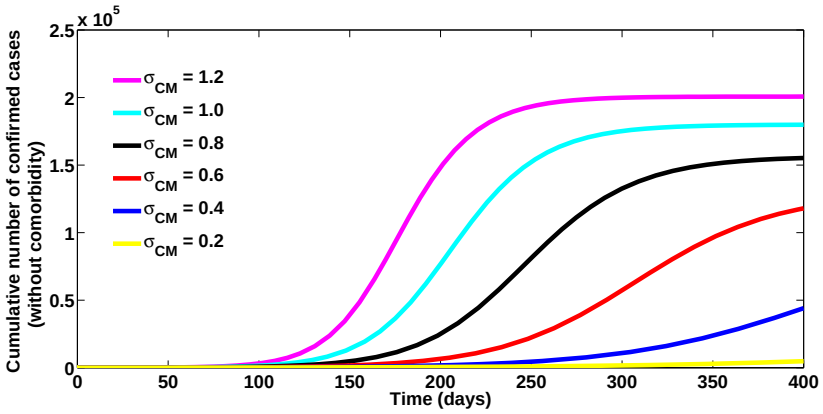

Figure 18: Simulations of the Cumulative number of confirmed cases (without comorbidity): effect of σ_{CM}

medRxiv preprint doi: https://doi.org/10.1101/2020.08.04.20168013; this version posted September 10, 2020. The copyright holder for this preprint **(which was not certified by peer review)** is the author/funder, who has granted medRxiv a license to display the preprint in perpetuity.
It is made available under a CC-BY-NC-ND 4.0 International license .

Figure 11 depicts the fitting of the model when the cumulative confirmed cases were used to fit the model. The figure showed that the co-infection model (1) fitted well to the Lagos COVID-19 data (daily cumulative confirmed cases).

The projection of the cumulative confirmed cases, depicted in Figure 12, shows that in the absence of any preventive controls, the cumulative confirmed cases (including those co-infected with comorbidity) may reach 800,000 cases after 200 days (counting from the onset of infection in Lagos). As presented in Figure 13, the cumulative confirmed cases (including those with comorbidity) may gey up 900,000 cases after 200 days if the parameter accounting for hyper vulnerability of comorbid susceptibles is as high as 1.2 per day. The simulations of the cumulative confirmed cases (without comorbidity) may get up to 180,000 after 200 days, if the hyper susceptibility rate of comorbid susceptibles is as high as 1.2 per day (as depicted by Figure 14). However, this number decreases as efforts are strictly enforced to prevent COVID-19 infection among comorbid susceptibles, through the use of face-masks, observance of social distancing regulations. As illustrated in Figure 15, the cumulative confirmed cases (including those co-infected with comorbidity) may be as high as 1000,000 cases by the end of November, 2020 if the re-infection rates for COVID-19 is 0.1 per day. it may be worse than this if the re-infection rates increase higher. Similar conclusions are obtained when the cumulative confirmed cases (without comorbidity) are simulated at different re-infection rates, as depicted in Figure 16. When the cumulative confirmed cases with or without comorbidity are simulated at different infectivity levels for co-infected individuals (as presented in Figures 17 and 18), it is observed that the cumulative confirmed cases decreases with decreasing infectivity level for co-infected individuals.

The contour plot of the reproduction number $\mathcal{R}_{0c}$ with detection rate for singly infected individuals (η_1) and detection rate for co-infected individuals (η_2), shown in Figure 19, reveal that if the detection rate for infected individuals co-infected with comorbidity can be increased to about 0.7 per day and the detection rate for infected individuals (without comorbidites) kept at 0.3 per day, then the reproduction number $\mathcal{R}_{0c}$ can be brought below unity and COVID-19 infection eliminated from the population. The contour plot of the reproduction number, $\mathcal{R}_{0c}$, as a function of detection rate for singly infected individuals (η_1) and the modification parameter for high suscptibility of comorbid susceptibles, depicted in Figure 20 shows that if policies are strictly put in place to step down the probability of COVID-19 infection by comorbid susceptibles to as low as 0.4 per day and step up the detection rate for singly infected individuals to 0.7 per day, then the reproduction number can be brought very low below one, and COVID-19 infection eliminated from the population.

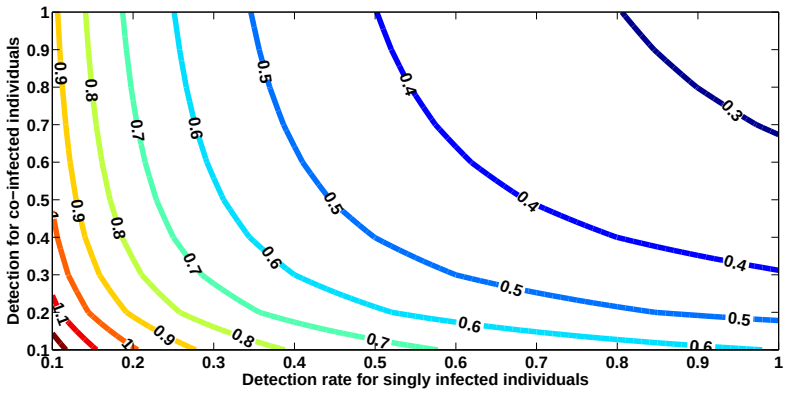

Figure 19: A contour plot of $\mathcal{R}_{0c}$ as a function of detection rate for singly infected individuals (η_1) and detection rate for co-infected individuals (η_2)

medRxiv preprint doi: https://doi.org/10.1101/2020.08.04.20168013; this version posted September 10, 2020. The copyright holder for this preprint **(which was not certified by peer review)** is the author/funder, who has granted medRxiv a license to display the preprint in perpetuity.
It is made available under a CC-BY-NC-ND 4.0 International license .

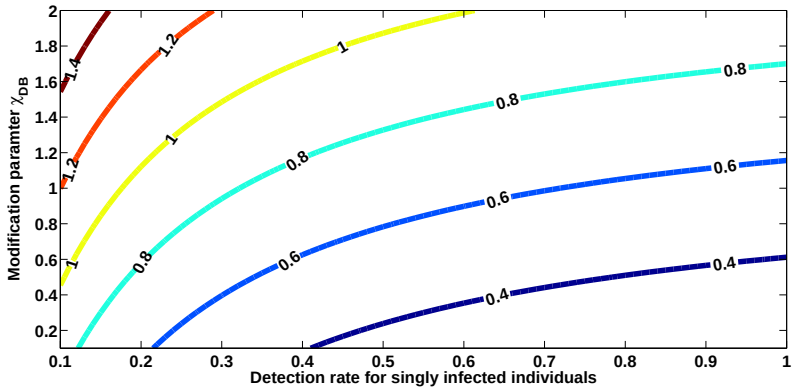

Figure 20: A contour plot of $\mathcal{R}_{0c}$ as a function of detection rate for singly infected individuals (η_1) and the modification parameter for high susceptibility of those with comorbidity (χ_{CM})

medRxiv preprint doi: https://doi.org/10.1101/2020.08.04.20168013; this version posted September 10, 2020. The copyright holder for this preprint (which was not certified by peer review) is the author/funder, who has granted medRxiv a license to display the preprint in perpetuity.
It is made available under a CC-BY-NC-ND 4.0 International license .

5 Analysis of the optimal control model

The Pontryagin's Maximum Principle shall be applied, in this section, to determine the necessary conditions for the optimal control of the model. We incorporate time dependent controls into the model (1) to determine the optimal strategy for controlling the spread of COVID-19. Thus, we have,

$$\begin{aligned}
\frac{dS_{\text{H}}}{dt} &= \Lambda_{\text{H}} - (\lambda_{\text{CV}} + \theta_{\text{CM}} + \mu_{\text{H}})S_{\text{H}} \\
\frac{dS_{\text{HCM}}}{dt} &= \theta_{\text{CM}}S_{\text{H}} - (1-u_1)\chi_{\text{CM}}\lambda_{\text{CV}}S_{\text{HCM}} - \mu_{\text{H}}S_{\text{HCM}} \\
\frac{dI_{\text{CV}}}{dt} &= \lambda_{\text{CV}}S_{\text{H}} - (u_2\eta_1 + \varphi_{\text{I1}} + \mu_{\text{H}})I_{\text{CV}} + (1-u_3)\psi_1\lambda_{\text{CV}}R_{\text{CV}} \\
\frac{dQ_{\text{CV}}}{dt} &= u_2\eta_1 I_{\text{CV}} - (\varphi_{\text{Q1}} + \delta_1 + \mu_{\text{H}})Q_{\text{CV}} \\
\frac{dR_{\text{CV}}}{dt} &= \varphi_{\text{I1}}I_{\text{CV}} + \varphi_{\text{Q1}}Q_{\text{CV}} - \mu_{\text{H}}R_{\text{CV}} - (1-u_3)\psi_1\lambda_{\text{CV}}R_{\text{CV}} \\
\frac{dI_{\text{CVCM}}}{dt} &= (1-u_1)\chi_{\text{CM}}\lambda_{\text{CV}}S_{\text{HCM}} - (u_2\eta_2 + \varphi_{\text{I2}} + \mu_{\text{H}})I_{\text{CVCM}} + (1-u_3)\psi_2\lambda_{\text{CV}}R_{\text{CM}} \\
\frac{dQ_{\text{CVCM}}}{dt} &= u_2\eta_2 I_{\text{CVCM}} - (\delta_1 + \delta_2 + \varphi_{\text{Q2}} + \mu_{\text{H}})Q_{\text{CVCM}} \\
\frac{dR_{\text{CM}}}{dt} &= \varphi_{\text{I2}}I_{\text{CVCM}} + \varphi_{\text{Q2}}Q_{\text{CVCM}} - \mu_{\text{H}}R_{\text{CM}} - (1-u_3)\psi_2\lambda_{\text{CV}}R_{\text{CM}}
\end{aligned} \tag{16}$$

subject to the initial conditions
$S_{\text{H}}(0) = S^0_{\text{H}}, S_{\text{HCM}}(0) = S^0_{\text{HCM}}, I_{\text{CV}}(0) = I^0_{\text{CV}}, Q_{\text{CV}}(0) = Q^0_{\text{CV}}, R_{\text{CV}}(0) = R^0_{\text{CV}}, I_{\text{CVCM}}(0) = I^0_{\text{CVCM}}, Q_{\text{CVCM}}(0) = Q^0_{\text{CVCM}}, R_{\text{CM}}(0) = R^0_{\text{CM}}$

with

$$\lambda_{\text{CV}} = \frac{\beta_{\text{CV}}(I_{\text{CV}} + \sigma_{\text{CM}}I_{\text{CVCM}})}{N_{\text{H}}},$$

The control functions, $u_1(t), u_2(t)$, and $u_3(t)$ are bounded, Lebesgue integrable functions. The control $u_1(t)$ represents the efforts geered towards preventing incident COVID-19 infections by comorbid suceptible humans. The control $u_2(t)$ is the effort aimed at intensifying detection of COVID-19 cases. Efforts aimed at preventing re-infection by those who have fully recovered from COVID-19 is represented by $u_3(t)$. The control u_1 satisfies $0 \leq u_1 \leq 0.9$, the controls u_2 and u_3 satisfy $0 < u_2, u_3 \leq 1$. The optimal control system examines scenarios where the number of infectious cases and the cost of implementing the controls $u_1(t), u_2(t)$, and $u_3(t)$ are minimized subject to the state system (16). For this, we consider the objective functional

$$J\big[u_1, u_2, u_3\big] = \int_0^T \big[I_{\text{CV}}(t) + I_{\text{CVCM}}(t) + \frac{B_1}{2}u_1^2 + \frac{B_2}{2}u_2^2 + \frac{B_3}{2}u_3^2\big]dt \tag{17}$$

T is the final time. We seek to find an optimal control, u_1^*, u_2^*, u_3^*, such that

$$J(u_1^*, u_2^*, u_3^*) = min\{J(u_1^*, u_2^*, u_3^*)|u_1, u_2, u_3 \in U\} \tag{18}$$

where $U = \{(u_1^*, u_2^*, u_3^*)\}$ such that u_1^*, u_2^*, u_3^* are measurable with $0 \leq u_1^* \leq 1, 0 \leq u_2^* \leq 1, 0 \leq u_3^* \leq 1$, for $t \in [0, T]$ is the control set. The Pontryagin's Maximum Principle [37] gives the necessary conditions which an optimal control pair must satisfy. This principle transforms (16), (17) and (18) into a problem

medRxiv preprint doi: https://doi.org/10.1101/2020.08.04.20168013; this version posted September 10, 2020. The copyright holder for this preprint (which was not certified by peer review) is the author/funder, who has granted medRxiv a license to display the preprint in perpetuity.
It is made available under a CC-BY-NC-ND 4.0 International license .

of minimizing a Hamiltonian, $\mathcal{H}$, pointwisely with regards to the control functions, u_1, u_2, u_3:

$$\begin{aligned}\mathcal{H} = {} & I_{\text{CV}}(t) + I_{\text{CVCM}}(t) + \frac{B_1}{2}u_1^2 + \frac{B_2}{2}u_2^2 + \frac{B_3}{2}u_3^2 \\ & + \lambda_{S_{\text{H}}}\left[\Lambda_{\text{H}} - ((1-u_1)\lambda_{\text{CV}} + \theta_{\text{CM}} + \mu_{\text{H}})S_{\text{H}}\right] \\ & + \lambda_{S_{\text{HCM}}}\left[\theta_{\text{CM}}S_{\text{H}} - (1-u_2)\chi_{\text{CM}}\lambda_{\text{CV}}S_{\text{HCM}} - \mu_{\text{H}}S_{\text{HCM}}\right] \\ & + \lambda_{I_{\text{CV}}}\left[(1-u_1)\lambda_{\text{CV}}S_{\text{H}} - (u_3\eta_1 + \varphi_{\text{I1}} + \mu_{\text{H}})I_{\text{CV}} + (1-u_4)\psi_1\lambda_{\text{CV}}R_{\text{CV}}\right] \\ & + \lambda_{Q_{\text{CV}}}\left[u_3\eta_1 I_{\text{CV}} - (\varphi_{\text{Q1}} + \delta_1 + \mu_{\text{H}})Q_{\text{CV}}\right] \\ & + \lambda_{R_{\text{CV}}}\left[\varphi_{\text{I1}}I_{\text{CV}} + \varphi_{\text{Q1}}Q_{\text{CV}} - \mu_{\text{H}}R_{\text{CV}} - (1-u_4)\psi_1\lambda_{\text{CV}}R_{\text{CV}}\right] \\ & + \lambda_{I_{\text{CVCM}}}\left[(1-u_2)\chi_{\text{CM}}\lambda_{\text{CV}}S_{\text{HCM}} - (u_3\eta_2 + \varphi_{\text{I2}} + \mu_{\text{H}})I_{\text{CVCM}} + (1-u_4)\psi_2\lambda_{\text{CV}}R_{\text{CM}}\right] \\ & + \lambda_{Q_{\text{CVCM}}}\left[u_3\eta_2 I_{\text{CVCM}} - (\delta_1 + \delta_2 + \varphi_{\text{Q2}} + \mu_{\text{H}})Q_{\text{CVCM}}\right] \\ & + \lambda_{R_{\text{CM}}}\left[\varphi_{\text{I2}}I_{\text{CVCM}} + \varphi_{\text{Q2}}Q_{\text{CVCM}} - \mu_{\text{H}}R_{\text{CM}} - (1-u_4)\psi_2\lambda_{\text{CV}}R_{\text{CM}}\right]\end{aligned} \tag{19}$$

Theorem 5.1 *For an optimal control set u_1, u_2, u_3 that minimizes J over U , there are adjoint variables, $\lambda_1, \lambda_2, ..., \lambda_8$ satisfying*

$$-\frac{\partial \lambda_i}{\partial t} = \frac{\partial \mathcal{H}}{\partial i}$$

and with transversality conditions

$$\lambda_i(t_f) = 0, \qquad where, \quad i = S_{\text{H}}, S_{\text{HCM}}, I_{\text{CV}}, Q_{\text{CV}}, R_{\text{CV}}, I_{\text{CVCM}}, Q_{\text{CVCM}}, R_{\text{CM}}. \tag{20}$$

Furthermore,

$$\begin{aligned} u_1^* &= max\left\{0, min\left(1, \frac{(\lambda_2 - \lambda_6)\beta_{\text{CV}}\chi_{\text{CM}}S_{\text{CM}}(I_{\text{CV}} + \sigma_{\text{CM}}I_{\text{CVCM}})}{B_1 N_{\text{H}}}\right)\right\}, \\ u_2^* &= max\left\{0, min\left(1, \frac{(\lambda_3 - \lambda_4)I_{\text{CV}}\eta_1 + (\lambda_6 - \lambda_7)I_{\text{CVCM}}\eta_2}{B_2}\right)\right\}, \\ u_3^* &= max\left\{0, min\left(1, \frac{(\lambda_3 - \lambda_5)\beta_{\text{CV}}R_{\text{CV}}(I_{\text{CV}} + \sigma_{\text{CM}}I_{\text{CVCM}}) + (\lambda_6 - \lambda_8)\beta_{\text{CV}}R_{\text{CM}}(I_{\text{CV}} + \sigma_{\text{CM}}I_{\text{CVCM}})}{B_3 N_{\text{H}}}\right)\right\}, \end{aligned} \tag{21}$$

Proof of Theorem 5.1
Suppose $U^* = (u_1^*, u_2^*, u_3^*)$ is an optimal control and $S_{\text{H}}^*, S_{\text{HCM}}^*, I_{\text{CV}}^*, Q_{\text{CV}}^*, R_{\text{CV}}^*, I_{\text{CVCM}}^*, Q_{\text{CVCM}}^*, R_{\text{CM}}^*$ are the corresponding state solutions. Applying the Pontryagin's Maximum Principle [37], there exist adjoint variables satisfying:

$$\begin{aligned} & -\frac{d\lambda_{S_{\text{H}}}}{dt} = \frac{\partial \mathcal{H}}{\partial S_{\text{H}}}, \quad \lambda_{S_{\text{H}}}(t_f) = 0, \quad -\frac{d\lambda_{S_{\text{HCM}}}}{dt} = \frac{\partial \mathcal{H}}{\partial S_{\text{HCM}}}, \quad \lambda_{S_{\text{HCM}}}(t_f) = 0, \quad -\frac{d\lambda_{I_{\text{CV}}}}{dt} = \frac{\partial \mathcal{H}}{\partial I_{\text{CV}}}, \quad \lambda_{I_{\text{CV}}}(t_f) = 0, \\ & -\frac{d\lambda_{Q_{\text{CV}}}}{dt} = \frac{\partial \mathcal{H}}{\partial Q_{\text{CV}}}, \quad \lambda_{Q_{\text{CV}}}(t_f) = 0, -\frac{d\lambda_{R_{\text{CV}}}}{dt} = \frac{\partial \mathcal{H}}{\partial R_{\text{CV}}}, \quad \lambda_{R_{\text{CV}}}(t_f) = 0, \quad -\frac{d\lambda_{I_{\text{CVCM}}}}{dt} = \frac{\partial \mathcal{H}}{\partial I_{\text{CVCM}}}, \quad \lambda_{I_{\text{CVCM}}}(t_f) = 0, \end{aligned} \tag{22}$$

with transversality conditions;
$\lambda_{S_{\text{H}}}(t_f) = \lambda_{S_{\text{HCM}}}(t_f) = \lambda_{I_{\text{CV}}}(t_f) = \lambda_{Q_{\text{CV}}}(t_f) = \lambda_{R_{\text{CV}}}(t_f) = \lambda_{I_{\text{CVCM}}}(t_f) = \lambda_{Q_{\text{CVCM}}}(t_f) = \lambda_{R_{\text{CM}}}(t_f) = 0$ We can determine the behaviour of the control by differentiating the Hamiltonian, $\mathcal{H}$ with respect to the controls(u_1, u_2, u_3) at t. On the interior of the control set, where $0 < u_j < 1$ for all $(j = 1, 2, 3)$, we obtain

$$\begin{aligned} 0 &= \frac{\partial \mathcal{H}}{\partial u_1} = B_1 N_{\text{H}} u_1^* + (\lambda_2 - \lambda_6)\beta_{\text{CV}}S_{\text{CM}}(I_{\text{CV}} + \sigma_{\text{CM}}I_{\text{CVCM}}), \\ 0 &= \frac{\partial \mathcal{H}}{\partial u_2} = B_2 u_2^* + (\lambda_4 - \lambda_3)\eta_1 I_{\text{CV}} + (\lambda_7 - \lambda_6)\eta_2 I_{\text{CVCM}}, \\ 0 &= \frac{\partial \mathcal{H}}{\partial u_3} = B_3 N_{\text{H}} u_3^* + \beta_{\text{CV}}(I_{\text{CV}} + \sigma_{\text{CM}}I_{\text{CVCM}})R_{\text{CV}}(\lambda_5 - \lambda_3) + \beta_{\text{CV}}(I_{\text{CV}} + \sigma_{\text{CM}}I_{\text{CVCM}})R_{\text{CM}}(\lambda_8 - \lambda_6) \end{aligned} \tag{23}$$

Therefore, we have that [25]

medRxiv preprint doi: https://doi.org/10.1101/2020.08.04.20168013; this version posted September 10, 2020. The copyright holder for this preprint **(which was not certified by peer review)** is the author/funder, who has granted medRxiv a license to display the preprint in perpetuity.
It is made available under a CC-BY-NC-ND 4.0 International license .

$$
\begin{aligned}
u_1^* &= \frac{(\lambda_2-\lambda_6)\beta_{\text{CV}}\chi_{\text{CM}}S_{\text{CM}}(I_{\text{CV}}+\sigma_{\text{CM}}I_{\text{CVCM}})}{B_1N_{\text{H}}},\\
u_2^* &= \frac{(\lambda_3-\lambda_4)I_{\text{CV}}\eta_1+(\lambda_6-\lambda_7)I_{\text{CVCM}}\eta_2}{B_2},\\
u_3^* &= \frac{(\lambda_3-\lambda_5)\beta_{\text{CV}}R_{\text{CV}}(I_{\text{CV}}+\sigma_{\text{CM}}I_{\text{CVCM}})+(\lambda_6-\lambda_8)\beta_{\text{CV}}R_{\text{CM}}(I_{\text{CV}}+\sigma_{\text{CM}}I_{\text{CVCM}})}{B_3N_{\text{H}}},
\end{aligned}
\tag{24}
$$

$$
\begin{aligned}
u_1^* &= max\left\{0, min\left(1, \frac{(\lambda_2-\lambda_6)\beta_{\text{CV}}\chi_{\text{CM}}S_{\text{CM}}(I_{\text{CV}}+\sigma_{\text{CM}}I_{\text{CVCM}})}{B_1N_{\text{H}}}\right)\right\},\\
u_2^* &= max\left\{0, min\left(1, \frac{(\lambda_3-\lambda_4)I_{\text{CV}}\eta_1+(\lambda_6-\lambda_7)I_{\text{CVCM}}\eta_2}{B_2}\right)\right\},\\
u_3^* &= max\left\{0, min\left(1, \frac{(\lambda_3-\lambda_5)\beta_{\text{CV}}R_{\text{CV}}(I_{\text{CV}}+\sigma_{\text{CM}}I_{\text{CVCM}})+(\lambda_6-\lambda_8)\beta_{\text{CV}}R_{\text{CM}}(I_{\text{CV}}+\sigma_{\text{CM}}I_{\text{CVCM}})}{B_3N_{\text{H}}}\right)\right\},
\end{aligned}
\tag{25}
$$

medRxiv preprint doi: https://doi.org/10.1101/2020.08.04.20168013; this version posted September 10, 2020. The copyright holder for this preprint (which was not certified by peer review) is the author/funder, who has granted medRxiv a license to display the preprint in perpetuity.
It is made available under a CC-BY-NC-ND 4.0 International license .

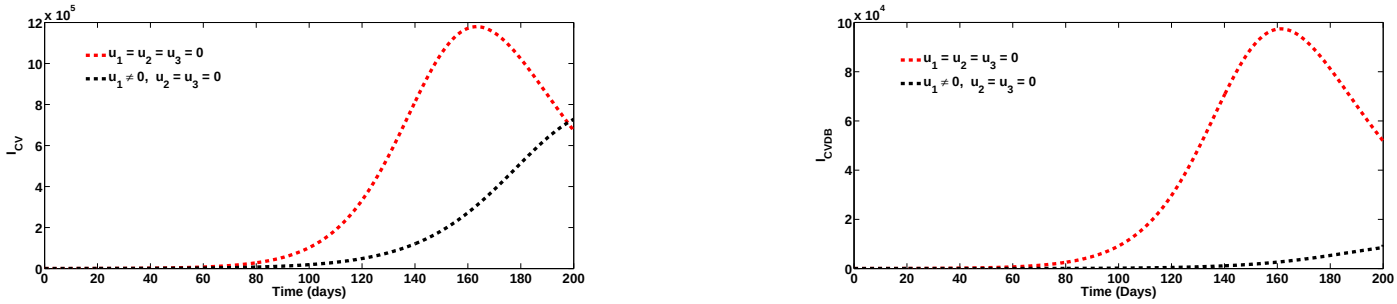

(a) (b)

Figure 21: Plots of the total number of COVID-19 infected individuals when strategy A is implemented ($u_1 \neq 0$). Here, $\beta_{cv} = 0.2001$, $\psi_1 = \psi_2 = 0.4$. All other parameters as in Table 1

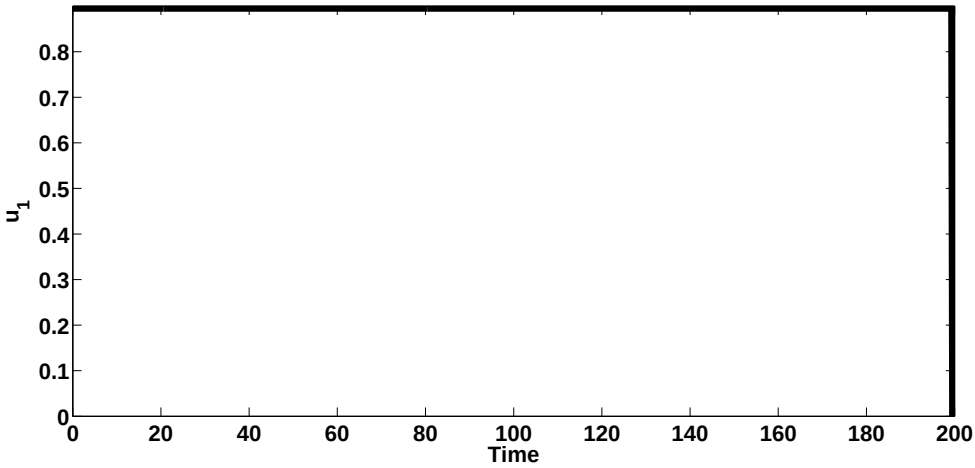

Figure 22: Control profile for the effect of the control u_1 on the dynamics of the model (1). Here, $\beta_{cv} = 0.2001$, $\psi_1 = \psi_2 = 0.4$. All other parameters as in Table 1

5.1 Strategy A: COVID-19 prevention among Comorbid susceptibles ($u_1 \neq 0$)

Simulations of the optimal control system when the strategy that prevents COVID-19 among comorbid susceptibles ($u_1 \neq 0$) is implemented, are presented in Figure 21. It is seen that when this intervention strategy is implemented, there is a significant decrease in the total number of individuals singly infected with COVID-19 (Figure 21(a)) and those co-infected with COVID-19 and comorbidity (Figure 21 (b)). Specifically, this strategy averts 908,500 new cases of COVID-19 and also prevents 94,747 new cases of co-infection of COVID-19 and comorbidity after 160 days. The control profile for this control strategy given in Figure 22 shows that control u_1 is at its peak throughout the entire simulation period.

5.2 Strategy B: Case detection control ($u_2 \neq 0$)

Simulations of the optimal control system when the case detection control ($u_2 \neq 0$) is implemented, are presented in Figure 23. It is seen that when this intervention strategy is implemented, there is a significant drop in the total number of individuals singly infected with COVID-19 and the co-infection cases. To be specific, this strategy averts 657,100 new COVID-19 cases after 160 days. The strategy also averts 67,230 new co-infection cases after 160 days. The control profile for this intervention control given in Figure 24 also shows that control u_2 is at its maximum value for the entire period of the simulation.

5.3 Strategy C: Control against COVID-19 re-infection ($u_3 \neq 0$)

Simulations of the optimal control system when control against COVID-19 re-infection ($u_3 \neq 0$) is implemented, are presented in Figure 25. It is observed that when this intervention strategy is applied, there is a significant reduction in the total number of individuals singly infected with COVID-19 and those co-infected with comorbidity. As a matter of fact, this strategy averts 431,300 new COVID-19 cases and

medRxiv preprint doi: https://doi.org/10.1101/2020.08.04.20168013; this version posted September 10, 2020. The copyright holder for this preprint **(which was not certified by peer review)** is the author/funder, who has granted medRxiv a license to display the preprint in perpetuity.
It is made available under a CC-BY-NC-ND 4.0 International license .

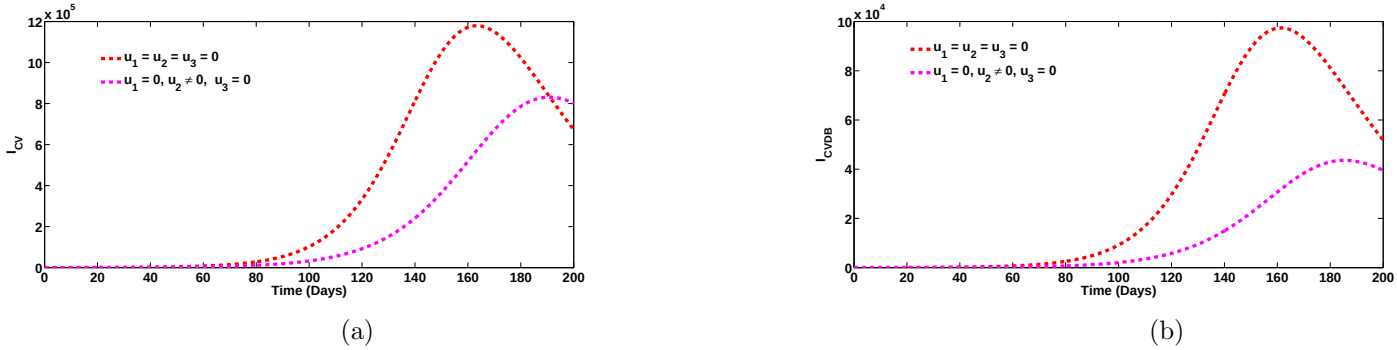

(a) (b)

Figure 23: Plots of the total number of COVID-19 infected individuals when strategy B is implemented ($u_2 \neq 0$). Here, $\beta_{\text{cv}} = 0.2001$, $\psi_1 = \psi_2 = 0.4$. All other parameters as in Table 1

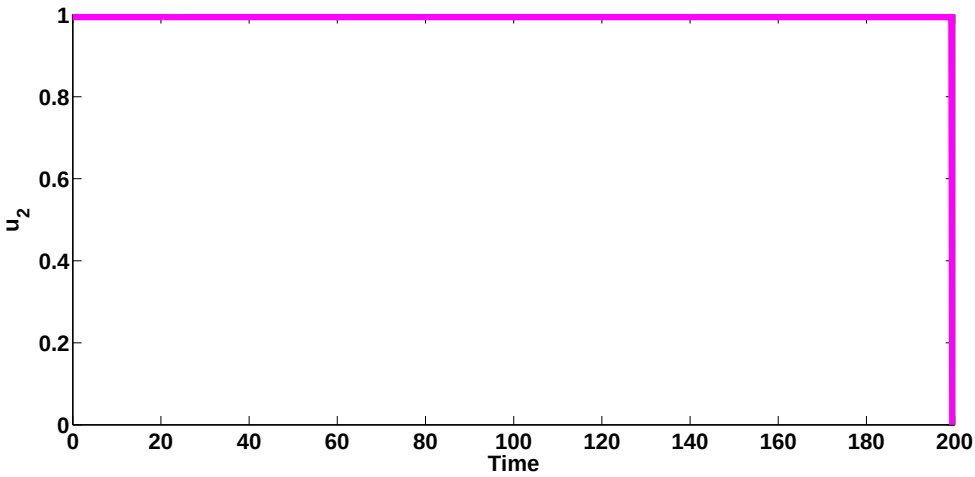

Figure 24: Control profile for the effect of the control u_2 on the dynamics of the model (1). Here, $\beta_{\text{cv}} = 0.2001$, $\psi_1 = \psi_2 = 0.4$. All other parameters as in Table 1

medRxiv preprint doi: https://doi.org/10.1101/2020.08.04.20168013; this version posted September 10, 2020. The copyright holder for this preprint (which was not certified by peer review) is the author/funder, who has granted medRxiv a license to display the preprint in perpetuity.
It is made available under a CC-BY-NC-ND 4.0 International license .

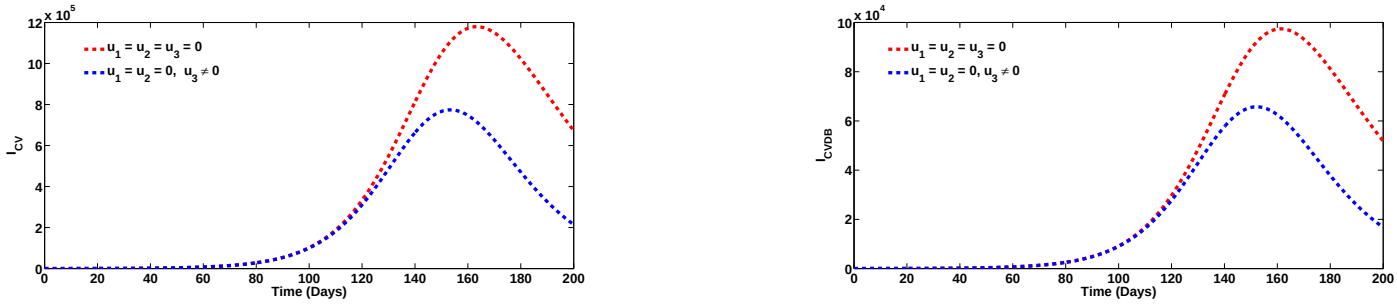

(a) (b)

Figure 25: Plots of the total number of COVID-19 infected individuals when strategy C is implemented ($u_3 \neq 0$). Here, $\beta_{\text{cv}} = 0.2001$, $\psi_1 = \psi_2 = 0.4$. All other parameters as in Table 1

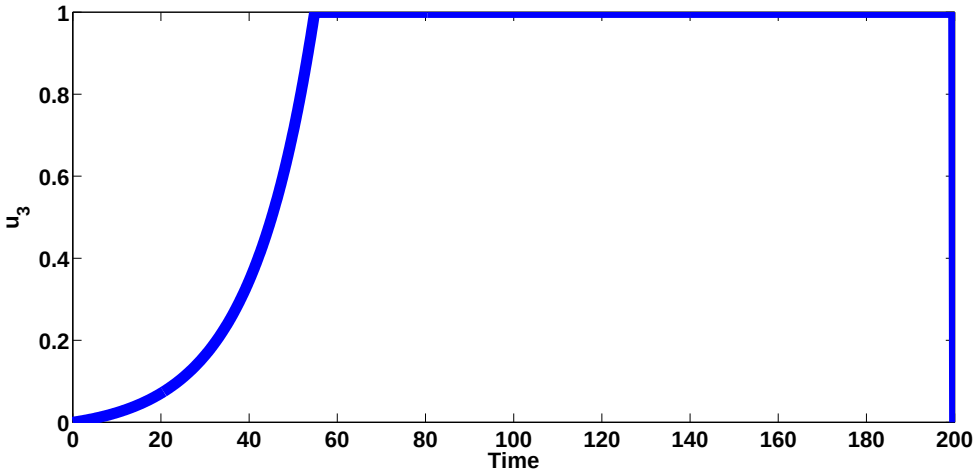

Figure 26: Control profile for the effect of the control u_3 on the dynamics of the model (1). Here, $\beta_{\text{cv}} = 0.2001$, $\psi_1 = \psi_2 = 0.4$. All other parameters as in Table 1

34,620 co-infection new cases. The control profile for this intervention control given in Figure 26 shows that control u_3 rises steadily to its maximum value in about 50 days and maintains this peak for the entire period of the simulation.

5.4 Cost-effectiveness analysis

The cost-effectiveness analysis is used to evaluate the health interventions related benefits in order to justify the costs of the strategies [7]. This is obtained by comparing the differences among the health outcomes and costs of those interventions; achieved by computing the incremental cost-effectiveness ratio (ICER), which is defined as the cost per health outcome.

We calculated the total number of cases averted and the total cost of the strategies applied in Table 4. The total number of cases prevented is obtained by calculating the total number of individuals when controls are implemented and the total number when control is not administered. In a similar manner, we apply the cost functions $\frac{1}{2}B_1u_1^2, \frac{1}{2}B_2u_2^2, \frac{1}{2}B_3u_3^2$, over time, to compute the total cost for the various strategies that were carried out. We assume the weight constants $B_1 = 400, B_3 = 500$ while $B_2 = 700$. We assumed here that, the cost of implementing the case detection control is much higher compared to the cost of implementing the preventive controls (which are mainly non-pharmaceutical). The cost-effectiveness of strategy C (control against re-infection by those who have recovered from a previous COVID-19 infection) and strategy B (case detection control) are now compared.

$$\text{ICER (C)} = \frac{500}{465,920} = 0.001073$$

$$\text{ICER (B)} = \frac{700 - 500}{724,330 - 465,920} = 0.000774$$

medRxiv preprint doi: https://doi.org/10.1101/2020.08.04.20168013; this version posted September 10, 2020. The copyright holder for this preprint (which was not certified by peer review) is the author/funder, who has granted medRxiv a license to display the preprint in perpetuity.
It is made available under a CC-BY-NC-ND 4.0 International license .

From ICER (C) and ICER(B), we observe a cost saving of 0.000774 observed for strategy B over strategy C. This implies that strategy C strongly dominated strategy B, showing that strategy C is more costly and less effective compared to strategy B. Therefore, strategy C is removed from subsequent ICER computations, shown in Table 5. We shall now compare strategies B and A. Comparing strategy B (case detection

Table 4: Increasing order of the total infection averted due to the control strategies

Strategy	**Total infection averted**	**Total cost**	ACER	ICER
C: $u_3(t)$	465, 920	500	0.001073	0.001073
B: $u_2(t)$	724, 330	700	0.000966	0.000774
A: $u_1(t)$	1,003, 247	400	0.0003987	-0.001076

Table 5: Increasing order of the total infection averted due to the control strategies

Strategy	**Total infection averted**	**Total cost**	ACER	ICER
B: $u_2(t)$	724, 330	700	0.000966	0.000966
A: $u_1(t)$	1,003, 247	400	0.0003987	-0.001076

control) and strategy A (control against COVID-19 infection by comorbid susceptibles), we observe that ICER (B) is greater than ICER (A), showing that strategy B strongly dominated strategy A and is more expensive and less effective compared to strategy A. Consequently, strategy A (the strategy that prevents COVID-19 infection by comorbid susceptibles) has the least ICER and is the most cost-effective of all the control strategies for the prevention of COVID-19. This also conforms with the results obtained from ACER method in Table 4 that strategy A is the most cost-effective strategy. It is also worthy of note to observe that this strategy averts more new COVID-19 cases than any other control strategy implemented.

$$\text{ICER (B)} = \frac{700}{724,330} = 0.000966$$

$$\text{ICER (A)} = \frac{400 - 700}{1,003,247 - 724,330} = -0.001076$$

medRxiv preprint doi: https://doi.org/10.1101/2020.08.04.20168013; this version posted September 10, 2020. The copyright holder for this preprint (which was not certified by peer review) is the author/funder, who has granted medRxiv a license to display the preprint in perpetuity.
It is made available under a CC-BY-NC-ND 4.0 International license .

6 Conclusion

In this work, we developed and analyzed a mathematical model for the dynamics of COVID-19 infection in order to assess the impacts of prior comorbidity on COVID-19 complications and COVID-19 re-infection. The model was simulated using data relevant to the dynamics of the diseases in Lagos, Nigeria, making predictions for the attainment of peak periods in the presence or absence of comorbidity. The model was shown to undergo the phenomenon of backward bifurcation which was caused by the parameter accounting for increased susceptibility to COVID-19 infection by comorbid susceptibles as well as the rate of re-infection by those who have recovered from a previous COVID-19 infection. The epidemiological interpretation of this phenomenon is that if recovery from COVID-19 does not confer lifelong immunity and efforts are not put in place to prevent COVID-19 infections by comorbid susceptible individuals, then the control of COVID-19 becomes difficult in the population, even when the associated reproduction number $\mathcal{R}_{0\text{C}} < 1$. Hence, it is recomended that efforts should be made by those in authority and policy makers to recommend preventive measures to curb COVID-19 infection by comorbid susceptibles and re-infection with COVID-19 so as to bring the burden of COVID-19 infection very low at the community level.

Sensivity analysis of the model when the population of individuals co-infected with COVID-19 and comorbidity is used as response function revealed that the top ranked parameters that drive the dynamics of the co-infection model are the effective contact rate for COVID-19 transmission, β_{CV}, the parameter accounting for increased sucseptibility to COVID-19 by comorbid susceptibles, χ_{CM}, the comorbidity development rate, θ_{CM}, the detection rate for singly infected and co-infected individuals, η_1 and η_2, as well as the recovery rate from COVID-19 for co-infected individuals, φ_{I2}. Simulations of the model reveal that the cumulative confirmed cases (without comorbidity) may get up to 180,000 after 200 days, if the hyper susceptibility rate of comorbid susceptibles is as high as 1.2 per day. Moreover, the cumulative confirmed cases (including those co-infected with comorbidity) may be as high as 1000,000 cases by the end of November, 2020 if the re-infection rates for COVID-19 is 0.1 per day. It may be worse than this if the re-infection rates increase higher. In addition, if policies were strictly put in place to step down the probability of COVID-19 infection by comorbid susceptibles to as low as 0.4 per day and the detection rate for singly infected individuals stepped up to 0.7 per day, then the reproduction number could be brought very low below unity, and COVID-19 infection eliminated from the population. Optimal control and cost effectiveness analysis of the model reveals that the strategy that prevents COVID-19 infection by comorbid susceptibles has the least ICER and is the most cost-effective of all the control strategies for the prevention of COVID-19.

medRxiv preprint doi: https://doi.org/10.1101/2020.08.04.20168013; this version posted September 10, 2020. The copyright holder for this preprint (which was not certified by peer review) is the author/funder, who has granted medRxiv a license to display the preprint in perpetuity.
It is made available under a CC-BY-NC-ND 4.0 International license .

References

[1] Atangana A, Modelling the spread of COVID-19 with new fractal-fractional operators: Can the lockdown save mankind before vaccination? Chaos Solitons Fractals 2020;136:109860.

[2] Bai Y, Yao L, Wei T, Tian F, Jin DY, Chen L, Wang M, Presumed asymptomatic carrier transmission of COVID-19, JAMA 2020.

[3] Blower SM, Dowlatabadi H, Sensitivity and uncertainty analysis of complex models of disease transmission: an HIV model, as an example, Int. Stat. Rev. 1994;2:229-243.

[4] BBC News, Coronavirus: The world in lockdown in maps and charts, 7 April 2020 *https://www.bbc.com/news/world-52103747*.

[5] BBC News, Coronavirus: South Korea confirms second wave of infections, available on https://www.bbc.com/news/world-asia-53135626.

[6] Bjorgul K, Novicoff WM, and Saleh KJ, Evaluating comorbidity in total hip and knee arthroplasty: available instruments, J Orthop Traumatol (2010) 11 (4) 203?209. https://doi.org/10.1007/s10195-010-0115-x PMID: 21076850 PMCID: 3014469

[7] S. B. Cantor, T. G. Ganiats, Incremental cost-effectiveness analysis: the optimal strategy depends on the strategy set. Clin. Epidemiol. 52 (1999) (6), 517-522.

[8] C. Castillo-Chavez and B. Song, Dynamical models of tuberculosis and their applications, Math. Biosci. Eng. 2 (2004) 361-404.

[9] Chen T-M, Rui J, Wang Q-P, Zhao Z-Y, Cui J-A, and Yin L, A mathematical model for simulating the phase-based transmissibility of a novel coronavirus, Infect. Dis. Pov. 2020:9:24. doi.org/10.1186/s40249-020-00640-3

[10] Centres for Disease Control and Prevention (CDC), Coronavirus Disease 2019 (COVID-19), Available on https://www.cdc.gov/coronavirus/2019-ncov/index.html.

[11] Cucinotta D, Vanelli M, WHO Declares COVID-19 a Pandemic, Acta Biomed 2020;91:1: 157-160. doi: 10.23750/abm.v91i1.9397

[12] Dong E, Du H, Gardner L, Coronavirus COVID-19 global Cases by Johns Hopkins CSSE, Lancet Infect. Dis. (2020) https://gisanddata.maps.arcgis.com/apps/opsdashboard/index.html/bda7594740fd40299423467b48e9ecf6.

[13] Egonmwan AO, Okuonghae D, Mathematical analysis of a tuberculosis model with imperfect vaccine, Int. J. Biomath. 2019;12(7):1950073.

[14] Euro News Debate, Beijing tightens controls as new coronavirus outbreak fans fear of second wave, available on https://www.euronews.com/2020/06/15/new-coronavirus-outbreak-in-china-fans-fears-of-second-wave.

[15] Dahiru T, Aliyu AA, Shehu AU, A Review of Population based Studies on Diabetes Mellitus in Nigeria, Sub-Saharan African Journal of Medicine 2016;3(2)

[16] Ferguson NM, Laydon D, Nedjati-Gilani G, Imai N, Ainslie K, Baguelin M, Bhatia S, Boonyasiri A, Cucunubá Z, Cuomo-Dannenburg G, et al., Impact of Non-Pharmaceutical Interventions (NPIs) to Reduce COVID-19 Mortality and Healthcare Demand, vol. 16, Imperial College COVID-19 Response Team, London, 2020.

[17] Hethcote HW, The mathematics of infectious diseases, SIAM Rev. 2000;42(4):599-653.

[18] Huang C, Wang Y, Li X, Ren L, Zhao J, Hu Y, et al. Clinical features of patients infected with 2019 novel coronavirus in Wuhan, China. Lancet 2020;395:497-506.

medRxiv preprint doi: https://doi.org/10.1101/2020.08.04.20168013; this version posted September 10, 2020. The copyright holder for this preprint (which was not certified by peer review) is the author/funder, who has granted medRxiv a license to display the preprint in perpetuity.
It is made available under a CC-BY-NC-ND 4.0 International license .

[19] Ivorra B, Ferrandez MR, Vela-Perez M, Ramos AM, Mathematical modeling of the spread of the coronavirus disease 2019 (COVID-19) taking into account the undetected infections. The case of China, Commun. Nonlinear Sci. Numer. Simulat. 2020;88:105303.

[20] Khan MA, Atangana A, Modeling the dynamics of novel coronavirus (2019-nCov) with fractional derivative, Alexandria Engr. J., 2020. doi.org/10.1016/j.aej.2020.02.033

[21] Kucharski AJ, Russell TW, Diamond C, Liu Y, Edmunds J, Funk S, Eggo RM, Sun F, Jit M, Munday JD, et al., Early dynamics of transmission and control of COVID-19: A mathematical modelling study, Lancet Infect. Dis. 2020.

[22] Lai C-C, Wang C-Y, Hsueh P-R, Co-infections among patients with COVID-19: The need for combination therapy with non-anti-SARS-CoV-2 agents?, Journal of Microbiology, Immunology and Infection, https://doi.org/10.1016/j.jmii.2020.05.013

[23] Lakshmikantham, S., Leela, S., and Martynyuk, A. A., Stability Analysis of Nonlinear Systems, Marcel Dekker, Inc., New York, 1989.

[24] La Salle J, Lefschetz S, The Stability of Dynamical Systems, SIAM, Philadelphia, 1976.

[25] Lenhart, S., Workman, J.T., Optimal Control Applied to Biological Models. Chapman & Hall, Boca Raton, (2007)

[26] Life Expectancy in Nigeria, Retrieved on 24th June, 2020 from https://www.worldometers.info/demographics/nigeria-demographics/#life-exp

[27] McCall J, Genetic algorithms for modelling and optimisation, J. Comput. Appl. Math. 2005;184:205-222

[28] Mizumoto K, Chowell G, Transmission potential of the novel coronavirus (COVID-19) onboard the Diamond Princess Cruises Ship, 2020, Infect. Dis. Model. 2020.

[29] The Nigeria Center for Disease Control, *https://covid19.ncdc.gov.ng* (2020)

[30] Nwankwo A, Okuonghae D, A Mathematical Model for the Population Dynamics of Malaria with a Temperature Dependent Control. Differ Equ Dyn Syst 2019. doi.org/10.1007/s12591-019-00466-y

[31] Okuonghae D, Backward Bifurcation of an Epidemiological Model with Saturated Incidence, Isolation and Treatment Functions. Qual. Theory Dyn. Syst. 2019;18:413-440. doi.org/10.1007/s12346-018-0293-0.

[32] Okuonghae D, Omame A, Analysis of a mathematical model for COVID-19 population dynamics in Lagos, Nigeria, Chaos Solitons Fractals 2020;139:110032

[33] Okoye JO, Attitudinal, regional and sex related vulnerabilities to COVID-19: Considerations for early flattening of curve in Nigeria, Med J Islam Repub Iran. 2020(13 Jun);34.61. https://doi.org/10.34171/mjiri.34.61

[34] Omame A, Okuonghae D, Umana RA, Inyama SC, Analysis of a co-infection model for HPV-TB, Appl. Math. Model. 2020;77:881-901.

[35] Omame A, Okuonghae D, Inyama SC, A mathematical study of a model for HPV with two high risk strains, in *Mathematics Applied to Engineering, Modelling, and Social Issues* Studies in Systems, Decision and Control 2020;200, F. Smith, H. Dutta and J. N. Mordeson (eds.)

[36] A. Omame, R. A. Umana, D. Okuonghae, S. C. Inyama, Mathematical analysis of a two-sex Human Papillomavirus (HPV) model, International Journal of Biomathematics, 11 (7) (2018)

[37] L.S. Pontryagin , V.G. Boltyanskii , R.V. Gamkrelidze, E.F. Mishchenko , The Mathematical Theory of Optimal Processes, Wiley, New York, 1962.

medRxiv preprint doi: https://doi.org/10.1101/2020.08.04.20168013; this version posted September 10, 2020. The copyright holder for this preprint (which was not certified by peer review) is the author/funder, who has granted medRxiv a license to display the preprint in perpetuity.
It is made available under a CC-BY-NC-ND 4.0 International license .

[38] 70% of dead COVID-19 patients had diabetes, TB, hypertension- Ehanire, Available on https://healthwise.punchng.com/70-of-dead-covid-19-patients-had-diabetes-tb-hypertension-ehanire/

[39] Sene N, SIR epidemic model with Mittag-Leffler fractional derivative. Chaos Solitons Fractals 2020;137:109833.

[40] Sene N, Stability analysis of the generalized fractional differential equations with and without exogenous inputs. J. Nonlinear Sci. Appl., 2019;12:562-572.

[41] Smith J. South Korea reports more recovered coronavirus patients testing positive again. Available from: https://www. reuters.com/article/us-health-coronavirus-southkorea/southkorea-reports-more-recovered-coronavirus-patients-testingpositive- again-idUSKCN21V0JQ

[42] Tang B, Bragazzi NL, Li Q, Tang S, Xiao Y, Wu J, An updated estimation of the risk of transmission of the novel coronavirus (2019-nCov), Infect. Dis. Model. 2020;5:248-255

[43] Umana RA, Omame A, and Inyama SC, Deterministic and Stochastic Models of the Dynamics of Drug Resistant Tuberculosis; FUTO J. Ser. 2016;2(2):173-194.

[44] van den Driessche P, Watmough J, Reproduction numbers and sub-threshold endemic equilibria for compartmental models of disease transmission, Math. Biosci. 2002;180:29-48.

[45] World Population Review, *Lagos Population 2020 (Demographics, Maps, Graphs)*, Retrieved on 25th April, 2020 from https://worldpopulationreview.com/world-cities/lagos-population/.

[46] Wang D, Hu B, Hu C, Zhu F, Liu X, Zhang J, et al. Clinical characteristics of 138 hospitalized patients with 2019 novel coronavirus-infected pneumonia in Wuhan, China. JAMA 2020;323:1061-9.

[47] Woelfel R, Corman VM, Guggemos W, et al Clinical presentation and virological assessment of hospitalized cases of coronavirus disease 2019 in a travel-associated transmission cluster,. medRXiv March 8, 2020

[48] WHO,"No evidence that recovered COVID-19 patients cannot be reinfected", available on https://news.un.org/en/story/2020/04/1062612.

[49] Yanga J, Zheng Y, Gou X, Pu K, Chen Z, Guo Q, Ji R, Wang H, Wang Y, Zhou Y, Prevalence of comorbidity and its effects in patients infected with SARS-CoV-2: a systematic review and meta-analysis, Int. J. Infect. Dis. 2020;94:91-95